UNIVERSITY OF CALIFORNIA, SAN DIEGO

The role of the AMPK-GIV interaction in epithelial cell polarity

A thesis submitted in partial satisfaction of the

requirements for the degree Master of Science

in

Biology

by

Arjun Anit Patel

Committee in charge:

Professor Pradipta Ghosh, Chair
Professor Jens Lykke-Andersen, Co-chair
Professor Steven Wasserman

2015

The thesis of Arjun Anit Patel is approved and it is acceptable in quality and form for publication on microfilm and electronically:

Co-chair

Chair

University of California, San Diego

2015

TABLE OF CONTENTS

LIST OF FIGURES

LIST OF TABLES

ACKNOWLEDGEMENTS

I would like to thank Dr. Pradipta Ghosh and Dr. Nicolas Aznar for their excellent mentorship, encouragement, and enthusiasm throughout this project. I greatly appreciate the opportunity that Dr. Ghosh provided me by allowing me to join this lab. Additionally, I value the time and effort that both Dr. Ghosh and Dr. Aznar spent training me at the desk and at the lab bench. I am definitely a better scientist now compared to before I joined this lab, and I truly believe my experiences here will benefit me in the future.

I would also like to thank the rest of the Ghosh Lab for their support. I have really enjoyed working alongside and getting to know my colleagues in this lab.

I would like to thank the members of my thesis committee, Dr. Jens Lykke-Andersen and Dr. Steven Wasserman, as well.

Finally, I would like to thank my family for their continued encouragement and support through my time in this program.

The Results section is currently being prepared for submission for publication. Dr. Pradipta Ghosh and Dr. Nicolas Aznar have served as co-authors; the thesis author was the primary investigator and author of this material. I would like to thank Dr. Aznar for contributing data to Figures 1, 3, 5, 6, 7, 9, and 10.

ABSTRACT OF THE THESIS

The role of the AMPK-GIV interaction in epithelial cell polarity

by

Arjun Anit Patel

Master of Science in Biology

University of California, San Diego

Professor Pradipta Ghosh, Chair
Professor Jens Lykke-Andersen, Co-chair

Cell polarity is fundamental for the architecture and function of epithelial tissues. Epithelial polarization requires coordination of multiple fundamental cell processes, whose integration in space and time dictates overall epithelial morphogenesis. Loss of epithelial polarity not only impacts organ development and function, but also causes cancers. Here we identify Gα-Interacting Vesicle-associated protein (GIV; a.k.a. Girdin) as a novel substrate of AMPK, whose phosphorylation at a single site (Ser 245) is required for the stabilization of tight junctions (TJs) in polarized epithelial cells. Expression of a nonphosphorylatable GIV mutant S245→A made cells highly susceptible to energetic

stress or low calcium conditions, triggering early disassembly and impaired reassembly of functional TJs. By contrast, expression of phosphomimetic mutant (S245→D) made epithelial cells relatively resistant to energetic stress or low calcium conditions. Phosphorylation of GIV at S245 was also essential for epithelial morphogenesis. Furthermore, we show that an oncogenic mutant (L249→P) of GIV impairs AMPK-dependent phosphorylation of GIV at S245 and recapitulated the phenotypes of cells expressing the non-phosphorylatable S245→A mutant. More importantly, expression of either S245A or L249P mutants preferentially triggered anchorage-independent growth and transformation, whereas the expression of the constitutively phosphorylated S245D mutant restricted growth to an anchorage-dependent state. Taken together, we conclude that the AMPK-GIV axis stabilizes TJs, and that GIV is a key effector of AMPK at the TJs. This work illuminates a previously unforeseen mechanism by which metabolic stress may affect epithelial polarity, junctional integrity and epithelial morphogenesis via GIV, and how deregulation of this pathway may affect key growth properties of tumor cells.

INTRODUCTION

Epithelial cell polarity

Epithelial cells are common in the linings and surfaces of the body; for example, they are found in the gastrointestinal tract and epidermis of the skin. Epithelial cells normally display a polarized structure, with the membrane protein and organelle compositions differing between the basal and apical sides of the cell (Kaplan, Liu, & Tolwinski, 2009). It is this asymmetry between apical and basolateral compartments that segregates structures, proteins, and organellar functions across a cell. Epithelial polarity is a key element in cellular function, with roles in cell migration, mitosis, embryogenesis, and many other processes.

Asymmetric distribution of proteins and organelles is fundamentally important for epithelial homeostasis, development of organs/tissues and is essential for organ function in the human body. For example, in kidney and intestinal epithelial cells, the apical side is characterized by cilia and microvilli that help increase the surface area for molecule absorption. This apical side also contains receptors and adaptor proteins that initiate signal transduction pathways involved in growth and division, as well as actin and spectrin to provide cytoskeletal structure underneath the plasma membrane. The basal side contains different sets of proteins, such as the receptors integrin and dystroglycan, which connect the cytoskeleton to the extracellular matrix (ECM) and receive signals from the basement membrane environment to regulate adhesion and migration (Johnston & Ahringer, 2010).

Given its critical role in tissue homeostasis and organellar functions, loss of cell polarity is a key trigger for organ dysfunction via dysregulation of cell growth and division. For example, many diseases resulting from depolarization exhibit cyst and tumor growth

in epithelial tissues, by disrupting fundamental epithelial functions (Stein, Wandinger-Ness, & Roitbak, 2002). Loss in polarity signaling pathways have also emerged as key triggers that herald cancer and fuel cancer progression (Martin-Belmonte & Perez-Moreno, 2012).

Research has shown that loss of cell polarity can result from different factors, such as aberrant oncogenic protein activity, abnormal growth factor signal pathway activation, and external or internal cell stressors. For example, the E6 oncogene which is activated in human papilloma virus (HPV)-infected cells induces proteasomal degradation of Dlg, a protein playing a crucial role in regulation of apical-basal cell polarity. Meanwhile, aberrant activation of ErbB2, a cell proliferation-stimulating receptor tyrosine kinase involved in ovarian and endometrial cancers, leads to dissociation of PAR3 from PAR6-aPKC complex, normally a key regulator of apical cell structure, resulting in disrupted cell polarity (Lee & Vasioukhin, 2008).

In addition, epithelial cells can lose adherence to a basal surface and neighboring cells due to metabolic stress, which changes the function of junctional proteins such as those that make up tight junctions and adherens junctions (Zhang, Li, Young, & Caplan 2006). These junctions are complexes of proteins that exist on the lateral side of each epithelial cell to connect adjacent cells and provide an impermeable barrier in the space between the cells. This change, paired with the loss of epithelial cell polarity, is associated with epithelial-mesenchymal transition (EMT), where an epithelial cell develops into a mesenchymal stem cell and displays anchorage-independence and invasive properties (Kalluri & Weinberg, 2009).

GIV, a novel multi-modular signal transducer that is essential for epithelial polarity

GIV (G-alpha interacting vesicle associated protein, also known as Girdin) is a guanine nucleotide exchange factor (GEF) signal transduction protein involved in multiple signaling pathways. A heterotrimeric G-protein is a guanine nucleotide-binding protein made up of an alpha, beta, and gamma subunit. G-proteins are usually associated with a membrane receptor and can be activated when the alpha subunit binds to GTP and deactivated when this subunit binds to GDP. A GEF causes GDP to be replaced with GTP on G-proteins, causing activation. The G-protein can then transduce signals received from receptors at the cell's plasma membrane and initiate a signaling cascade within the cell.

GIV has been shown to function in signal transmission from not only G-protein coupled receptors (GPCR), but also from receptor tyrosine kinases (RTK) such as insulin receptors and epidermal growth factor receptors (EGFR) (Ghosh, Garcia-Marcos, & Farquhar, 2011). As such, GIV is gaining importance as a mediator of cross-talk between different types of membrane receptors. GIV contains several key domains important for its functions. Its coiled-coil domain in the center of the protein is needed for homodimerization with other GIV molecules (Enomoto *et al*., 2005). The HOOK domain at its N-terminus is needed for interacting with microtubules. Within the C-terminal region, the Akt and Actin-binding domains allow GIV to trigger remodeling of the cytoskeleton and cell migration. Additionally, a plastic Src Homology 2-like (SH2) domain allows GIV to interacts with RTKs (Lin *et al*., 2014). The Gαi-binding domain and GEF region at the C-terminus allow GIV to integrate upstream signals from various growth factor receptors by interacting with G proteins (Ghosh, Garcia-Marcos, & Farquhar, 2011). GIV is involved in a number of cellular processes, including, but not limited to, actin remodeling and cell

migration (Enomoto *et al.*, 2005), mitogenic signaling (Ghosh *et al*., 2010), fibrogenic signaling (Lopez-Sanchez *et al*., 2014), and tumorigenesis (Ghosh, Garcia-Marcos, & Farquhar, 2011).

Multiple groups have recently shown that GIV regulates epithelial cell polarity and morphogenesis (Sasaki *et al.*, 2015; Houssin *et al*., 2015; Ichimiya *et al*., 2012). GIV's role in the maintenance of cell-cell junctions and cell polarity has thus far been linked to its ability to link G protein signaling to the polarity complex protein, PAR3 (Sasaki et al., 2015). Sasaki and colleagues have found that PAR3 upregulates GIV expression at the transcriptional level during periods of polarization in epithelial cells through activation of the transcription factor AP-2. In GIV depleted MDCK cells, tight junction formation is significantly delayed and membrane barrier function is decreased after calcium switch, as measured by transepithelial electrical resistance (TEER). (Sasaki *et al.*, 2015).

The PAR proteins: Master regulators of polarity

The PAR proteins are involved in regulating apical-basal cell polarity, in order to maintain asymmetry. The PAR3-PAR6-aPKC complex has been shown to regulate apical cell polarity. By phosphorylating PAR1, aPKC promotes the inhibition of PAR1 kinase activity in the apical region (Goldstein & Macara, 2010). Similarly, once phosphorylated by PAR4 (mammalian homologue LKB1), PAR1 phosphorylates PAR3 to inhibit the latter in the basolateral compartment of the cell. (Martin-Belmonte & Perez-Moreno, 2012).

AMPK: A key metabolic sensor and regulator of cell polarity

AMPK (5'AMP-activated protein kinase) is a metabolic sensor protein which is activated under energetic stress. AMPK is a heterotrimeric protein composed of a catalytic alpha subunit and beta and gamma regulatory subunits. When the intra-cellular ratio of AMP to ATP is increased, AMPK is activated and acts to increase the amount of available ATP (Zhang, Li, Young, & Caplan, 2006). AMPK activation occurs when AMP or ADP binds to its gamma subunit, causing a conformational change that exposes residue T172 for phosphorylation. An upstream kinase, such as the tumor suppressor LKB1 or the calcium-influx mediated CAMKK2, can phosphorylate AMPK at residue T172, activating the kinase (Mihaylova & Shaw, 2011). AMPK phosphorylates target substrates in order to inhibit cell proliferation and migration, promote catabolism and induce apoptosis if necessary. AMPK is also a known tumor suppressor, seemingly acting as an arm of LKB1 to prevent the development of cancer. AMPK phosphorylates and activates TSC in order to inhibit mTORC1, a driver of protein synthesis and proliferation. AMPK activity is regulated by the DNA damage checkpoint tumor suppressor p53 as well (Luo, Zang, & Guo, 2010).

Intrigued by LKB1's effects on polarity, Zheng and colleagues investigated the potential regulatory role in polarity of one of its key effectors, AMPK. They observed that AMPK was activated in epithelial cells in conditions of high calcium, which coincided with tight junction assembly and polarization. Moreover, knock down of AMPK catalytic α subunit has been shown to decrease tight junction assembly as indicated by a loss of TEER, a measure of paracellular ion flow that depends on tight junction stability. In parallel, when calcium-depleted media was used to induce tight junction disassembly, the

destabilization of junctions was rescued in cells incubated with AICAR, an AMPK activator (Zheng & Cantley, 2007).

While it is clear that AMPK plays a role in tight junction assembly and stability, it remains unknown how this kinase actually regulates tight junctions. More specifically, who or what might serve as an effector of AMPK at the junctions to maintain cell polarity has not yet been identified. We found striking similarities in GIV and AMPK mediated regulation of epithelial cell polarity, and decided to investigate if there was a relationship between these two proteins. In this work, we identify GIV as a novel substrate of AMPK in epithelial cells, and elucidate the role of the AMPK-GIV pathway in polarity.

MATERIALS AND METHODS

Construction of a 3D model of GIV interaction with the α-subunit of AMPK.

The homology model of the AMPKα-GIV complex was constructed using ICM comparative (homology) modeling procedure (Cardozo *et al*., 1995) using the structure of constitutively active Par1-MARK2 (a member of the AMPK family of kinase) in complex with the CagA protein encoded by pathologic strains of Helicobacter pylori (Nesic *et al*., 2010; PDB: 3IEC) as a template and guided by the GIV/AMPKα sequence alignment in **Fig 1**. The initial model was by assigning the backbone coordinates of both target molecules (AMPKα and GIV) to their counterparts in the template; this model was further refined using extensive sampling of residue side chains in internal coordinates and then additionally relaxed by full-atom local minimization in the presence of distance restraints maintaining the conserved hydrogen bonds and thus protein secondary structure and topology.

Culture of Cell Lines and glucose starvation

Parental Cos7, MDCK, NIH3T3 and DLD1 cell lines were obtained from ATCC and cultured at 37°C in a 5% CO_2 humidified incubator exactly as mandated by ATCC guidelines. Briefly, Cos7, NIH3T3 and MDCK cells were grown in Dulbecco's modified Eagle's medium (DMEM) supplemented with 10% fetal bovine serum (FBS) and 1% penicillin-streptomycin-glutamine. DLD1 cells were grown in Roswell Park Memorial Institute medium (RPMI) supplemented with 10% fetal bovine serum (FBS) and 1% penicillin-streptomycin-glutamine. Cells were passaged at 90-100% confluency using ATV.

Glucose starvation was done using DMEM with no FBS or Glucose. Cells were treated with 4 mM EGTA (Fisher Scientific) in the appropriate experiments.

Plasmid Transfection

Polyethylenimine (PEI) was used for all transient transfections performed in this work. The PEI reagent was mixed with media without FBS and plasmid DNA, then incubated for 20 minutes at room temperature prior to incubation with cells. Fresh media was added to cells grown to 80-90% confluency, and then the transfection mix was incubated with the cells for five hours. After this period of time, the media was aspirated and fresh media was added for continued culture of cells until their use in assays.

To generate MDCK and DLD1 cell lines stably expressing GIV-WT and various mutants, cells were first transiently transfected with p3x-FLAG-CMV-14-GIV plasmid DNA using Genejuice transfection reagent (EMD Millipore) as per manufacturers' protocol. Briefly, transfection was carried out using 100 ul of OptiMEM (Life Technologies) and 3 ul of Genejuice reagent per µg of plasmid DNA. This reagent-DNA mixture was incubated at room temperature for 20 minutes. Cells at 80-90% confluency on the day of transfection were fed fresh, complete media prior to the addition of the transfection mix. Media was once again changed to 10% FBS DMEM or RPMI the next day. At 48 h after transfection, antibiotic selection was initiated by the addition of 800 µg/mL G418 (a neomycin analog). Selection of cells was carried out with changing of media every 48 h until all cells in a non-transfected control exposed to 800 ug/mL G418 were dead and cells in the transfected wells had grown to 100% confluency. Selected cells stably expressing GIV were subsequently transferred to a new dish and maintained for 5-6 weeks in 800 ug/mL G418. The resultant multiclonal pool was subsequently maintained in

the presence of 500 μg/ml G418. GIV expression was verified by immunoblotting using anti-GIV antibody.

Cell Lysis

For whole cell lysates, cells were washed twice with cold 1x PBS, then harvested and centrifuged at 4°C to obtain a cell pellet. Cells were resuspended in lysis buffer (See Table 2) using a vortex and then boiled in an equal volume of 5x sample buffer (See Table 2). For immunoprecipitation and GST-pulldown experiments, cells were exposed to the same methods as in whole cell lysis, except that cells were resuspended in lysis buffer using a syringe.

Immunoprecipitation Assays

Immunoprecipitation Assays were performed as described before (Bhandari et al., 2015). Briefly, Cos7 cells grown on 10 cm plates were co-transfected with either GIV-FLAG constructs. After 48 h, cells were washed once with cold 1x PBS and harvested by scraping into 0.5 ml of IP buffer (20 mM HEPES pH 7.4, 5 mM Mg-acetate, 125 mM K-acetate, 0.4% Triton X-100, 1 mM DTT, 1x Complete Protease Inhibitor Cocktail (Roche), 1x Phosphatase Inhibitor Cocktails 1 & 2 (Sigma)) on ice. Cell lysates were incubated for 10 min at 4°C and centrifuged at 12,000×g for 10 min. Clarified cell lysates were incubated with anti-mouse FLAG-M2 antibody for 3 h at 4°C, followed by incubation with equilibrated protein G-Sepharose beads for 1 h at 4°C. Beads were washed thrice with cold IP buffer, eluted by heating at 95°C for 5 min in 1x Laemmli sample buffer, and bound proteins were analyzed by SDS-PAGE and immunoblotting.

Recombinant Protein Expression and Purification

Protein expression and purification was carried out as described previously

(Bhandari et al., 2015). Briefly, plasmids encoding GST-GIV-NT fusion constructs were used to express these proteins in *Escherichia coli* strain BL21 (DE3) (Invitrogen). Cells were grown in LB medium containing appropriate selection antibiotic at 37°C until an OD_{600} ~0.5-0.7, and protein expression was induced by adding 0.5 mM IPTG and growing cultures overnight at 25°C. Bacteria were pelleted from 500 ml of culture, re-suspended in 20 ml of lysis buffer (50 mM Tris-HCl pH 7.4, 100 mM NaCl, 10 mM $MgCl_2$, 5 mM EDTA, 2 mM DTT, 0.5% Triton X-100, 1x Complete Protease Inhibitor Cocktail (Roche), sonicated, and centrifuged to remove insoluble material. Affinity purification of solubilized proteins was carried out using glutathione-Sepharose 4B beads (GE Healthcare).

GST-pulldown

GST beads were mixed with GST-fused proteins and binding buffer (See Table 2; [50 mM Tris-HCl pH 7.4, 100 mM NaCl, 10 mM $MgCl_2$, 5 mM EDTA, 30 μM GDP, 2 mM DTT, 0.5% Triton X-100, 1x Complete Protease Inhibitor Cocktail (Roche)]), then rotated at 4°C overnight. GST beads were washed of residual solution the next day. After cell lysis, lysates were mixed with the GST beads and rotated at 4°C for 4 hours. Samples were washed four times in IP/GST-pulldown wash buffer (See Table 2). Proteins were then eluted using 5x sample buffer and boiling.

In vitro Kinase Assays

In vitro kinase assays were carried out as described previously (Bhandari et al., PNAS 2015) using purified His- or GST- tagged GIV-NT proteins (WT, L249P and S245A mutant; 3-5 μg/reaction) and commercially obtained recombinant, purified AMPK (Signal Chem; 100 ng/reaction). The reactions were started by addition of ATP (5 μCi/reaction γP^{32}-ATP and 6 μM cold ATP and carried out at 30°C in 30 μl of kinase buffer (20 mM

Tris·HCl pH 7.5, 2 mM EDTA, 10 mM $MgCl_2$, 0.1 mM AMP and 1 mM DTT). Phosphorylated proteins were separated on 12% SDS-PAGE and detected by autoradiography.

Immunoblot Analysis

Protein samples were separated by sodium dodecyl sulfate polyacrylamide gel electrophoresis (SDS-PAGE) in 1x running buffer (See Table 2) at 90-120 V until the proteins of interest were properly separated using a molecular weight standard marker (Precision Plus Protein All Blue Standard, Bio-Rad Laboratories, Inc.). Proteins were transferred from the gel to a methanol-activated PVDF membrane in the presence of 1x transfer buffer (See Table 2) at 30 V overnight. The following morning, an additional 120 V transfer for 15 minutes was performed. Membranes were blocked using 1x PBS with either 5% BSA (Sigma) for phosphorylated proteins or 5% dry nonfat milk for non-phosphorylated proteins. Membranes were incubated overnight in primary antibodies and washed with 1x PBST (1x PBS with 1:1000 dilution Tween-20). Membranes were then incubated in fluorescent secondary antibodies (See Table 1) for one hour, followed by further washes in 1x PBST and a final wash in 1x PBS. The Li-Cor Odyssey imaging system was used to detect and quantify two color channel fluorescent signals from the secondary antibodies.

Immunofluorescence

Cells grown on glass cover slips were fixed in 100% chilled methanol for 10 minutes at -20°C, then washed three times in 1x PBS. Next, cells were incubated in IF blocking buffer (See Table 2) on a rocker at room temperature for 30 minutes. Primary antibodies were then diluted in IF blocking buffer and cells were incubated with the

antibody solution in a humid chamber for one hour at room temperature. Cells were washed three times in 1x PBS and then incubated for one hour at room temperature with fluorescent secondary antibodies (See Table 1) which were diluted 1:500 in IF blocking buffer, along with DAPI at a 1:1000 dilution (Molecular Probes, Invitrogen). Cells were then washed three times in 1x PBS. Cell coverslips were placed over 6 ul of Prolong Gold antifade reagent (Invitrogen) on microscope slides. Images were acquired using a Leica CTR4000 Confocal Microscope at a 63x objective. Z-stack images were obtained by imaging approximately 4 um thick sections of cells in all channels. Cross-section images were obtained by automatic layering of individual slices from each Z-stack. Red-Green-Blue (RGB) graphic profiles were created by analyzing the distribution and intensity of pixels of those colors along a chosen line using ImageJ software.

Transepithelial Electrical Resistance [TEER]

Cells were seeded at a density of 1,000,000 cells/insert in 12 mm diameter Transwell inserts with a 0.4 um polyester membrane (Corning). Cells were grown in 10% FBS DMEM for three days, then resistance was measured with the Millicel-ERS resistance meter (Millipore) for control values. Cells were treated with 4 mM EGTA to induce stress and later 10% FBS DMEM for recovery; subsequent resistance recordings were taken at varying time points. All experiments were done using triplicates for each condition.

MDCK Cyst Formation Assay

The 3D collagen matrix procedure was performed as described previously (Bhandari et al., PNAS 2015). Briefly, $3x10^4$ MDCK cells were added to a collagen solution at pH 7 (GlutaMAX 24mM, NaHCO3 2.35 mg/ml, DMEM 1X FBS 2%, Hepes 20 mM, Collagen I 2 mg/ml) and placed in a well of a 4 well chamber slide. After the

collagen was polymerized, culture media (DMEM 1X FBS 2%) was added to the plate which was placed in a 37ºC CO_2 incubator. Media was changed every 2 days for up to 2 weeks. Cyst and tubule formations were monitored by phase-contrast microscopy.

Anchorage-dependent Colony Formation Assay

Anchorage-dependent growth was monitored on a solid (plastic) surface as described previously (Bhandari et al., PNAS 2015). Briefly, 5000 DLD1 cells stably expressing WT, S245D, S245A, and L249P GIV-FLAG constructs were grown in 6-well tissue culture plates at 37°C for 2 weeks in media supplemented with 0.2% FBS prior to staining with 0.1% crystal violet for 1 hour. Colonies were counted using "colony counter" application.

Anchorage-independent Growth Assay

Sterilized 1% agar in dH_2O was diluted in order to prepare matrix layers for this assay. 3 mL of warmed 0.5% agar diluted with 10% FBS RPMI was first pipetted into the bottom of each well of a 6-well plate. This base agar layer was allowed to set overnight at 4°C. DLD1 cells were passaged and counted, then 5,000 cells were seeded into a 3 mL mix of warmed 0.3% agar and 2% FBS RPMI. Plates were put into an incubator for 20-30 minutes to allow the top agar layer to set, then 2 mL warmed 2% FBS RPMI medium was added to each well. Plates were observed for growths over the course of 4 weeks, at which point they were incubated with 0.1% 3-(4,5-dimethylthiazol-2-yl)2 2,5-diphenyl tetrazolium bromide (MTT, Sigma) in PBS for 1 hour to visualize cells.

Ras-induced NIH3T3 Transformation Assay

NIH3T3 cells were transiently transfected with HA tagged K-Ras G12V and GIV-FLAG WT or mutants. Once confluent, cells were lifted from the plate with trypsin and

counted. Base agar composed on 0.5% agar and 10% FBS DMEM was prepared a day prior and stored at 4°C. 5,000 cells were then seeded into a mix of warmed 0.3% agar with 2% FBS DMEM. Plates were put into an incubator for 20-30 minutes to allow the top agar layer to set, then 2 mL warmed 2% FBS DMEM medium was added to each well. Plates were observed for growths over the course of 4 weeks, at which point they were incubated with 0.1% 3-(4,5-dimethylthiazol-2-yl)2 2,5-diphenyl tetrazolium bromide (MTT, Sigma) in PBS for 1 hour to visualize cells.

Statistical Analysis

Each experiment presented in the figures is representative of at least three independent experiments. Statistical significance between the differences of means was calculated by an unpaired student's t-test. A two tailed p value of <0.05 at 95% confidence interval is considered statistically significant. All graphical data presented were prepared using GraphPad or Matlab.

Table 1. Antibodies

Name	Isotype	Antigen	Dilution	Company
GIV phospho-S245	Rabbit polyclonal IgG	Short amino acid sequence around phosphorylated S245 of GIV	IB 1:250 IF 1:250	21st Century Biochemicals
Girdin CT (T-13)	Rabbit polyclonal IgG	C-terminal peptide from GIV of human origin	IB 1:500	Santa Cruz Biotechnology
Girdin coiled-coil region #13	Rabbit polyclonal IgG	GST-tagged recombinant protein from coiled-coil domain of GIV of rat origin	IB 1:500	EMD Millipore
Flag M2	Mouse monocolonal IgG	Eight amino acid peptide DYKDDDDK	IB 1:500 IP 2 ug per condition	Sigma Aldrich
Actin (C-11)-R	Rabbit polyclonal IgG	C-terminal peptide from Actin of human origin	IB 1:1000	Santa Cruz Biotechnology
Beta-tubulin	Mouse monocolonal IgG	Beta-tubulin derived from brain tissue of bovine origin	IB 1:500	Santa Cruz Biotechnology
Occludin	Mouse monocolonal IgG		IF 1:250	Zymed (Cat# 33-1500)
Beta-catenin	Mouse monocolonal IgG	Fusion protein consisting of the maltose binding protein fused to a 100 amino acid segment of the C-terminus of chicken Beta-catenin	IF 1:250	Invitrogen

Table 1. Antibodies, continued

Name	Isotype	Antigen	Dilution	Company
E-cadherin	Mouse monocolonal IgG	Raised against human breast carcinoma cell line T471	IF 1:50	Santa Cruz Biotechnology
Phospho-AMPK α T172	Rabbit polyclonal IgG	Synthetic phospho-peptide corresponding to residues surrounding T172 of human AMPK α	IB 1: 500	Cell Signaling Technology
AMPK α	Rabbit polyclonal IgG	Synthetic peptide corresponding to the amino-terminal sequence of human AMPK α	IB 1: 500	Cell Signaling Technology
Alexa Fluor 680 (Odyssey)	Rabbit IgG	F(ab')2 fragments	IB 1:10,000	Invitrogen Life Technologies
Alexa Fluor 800 (Odyssey)	Mouse IgG	F(ab')2 fragments	IB 1:10,000	Invitrogen Life Technologies
Alexa Fluor 594 GαR	Rabbit polyclonal IgG	F(ab')2 fragments	IF 1:500	Invitrogen Life Technologies
Alexa Fluor 488 GαM	Mouse monoclonal IgG	F(ab')2 fragments	IF 1:500	Invitrogen Life Technologies

Table 2. Buffers

Name	Components	Preparation	Origin
Lysis Buffer	20 mM Hepes pH 7.2, 125 mM K-acetate and 5 mM Mg-acetate	To 10 mL buffer, add 2 mM DTT, 1 tablet of Roche Protease inhibitor cocktail (Complete, EDTA free), 0.4% Triton X-100, 1X phosphatase inhibitor cocktail 2 and 3, 0.2 mM Sodium Orthovanadate	Made in lab
10x Running Buffer	0.25 M Tris, 1.92 M Glycine, 1% SDS, H_2O		Made in lab
10x Transfer Buffer	0.2 M Tris, 1.92 M Glycine, H_2O	Add 1 mL of 10% SDS to 1 L of 1X Transfer Buffer	Made in lab
5x Sample Buffer	5% SDS, 156 mM Tris, 25% glycerol, 0.025% Bromphenol Blue, 25% 2-Mercaptoethanol (BME), H_2O. pH 6.8	Add BME to aliquot prior to use	Made in lab
IF Blocking and Permeabilization Buffer	2 mg/mL BSA + 0.1% Triton-X in 1x PBS		Made in lab
IP/GST-pulldown Wash Buffer	1x PBS, 0.1% Tween 20, 5 mM EDTA, 10 mM $MgCl_2$, pH 7.4	Add 1M DTT at a 1:500 dilution and 100 mM Sodium Orthovanadate at a 1:500 dilution fresh before use	Made in lab
TNT Binding Buffer	50 mM Tris-HCl, 100 mM NaCl, 0.4% NP-40, 10 mM $MgCl_2$, 5 mM ETDA, pH 7.4	Add 1M DTT at a 1:500 dilution and 100 mM Sodium Orthovanadate at a 1:500 dilution fresh before use	Made in lab

Table 3. Plasmids

Construct	Vector	Gene	Origin
GIV-WT-3XFLAG	p3XFLAG-CMV-14	CCDC88a	Generated for this work
GIV-S245A-3XFLAG	p3XFLAG-CMV-14	CCDC88a	Generated for this work
GIV-S245D-3XFLAG	p3XFLAG-CMV-14	CCDC88a	Generated for this work
GIV-L249P-3XFLAG	p3XFLAG-CMV-14	CCDC88a	Generated for this work
GST-GIV-NT-WT (1-440)	pLIC GST	CCDC88a	Generated for this work (Ssp1)
GST-GIV-NT-WT (440-747)	pLIC GST	CCDC88a	Generated for this work (Ssp1)
GST-GIV-NT-S245A (1-440)	pLIC GST	CCDC88a	Generated for this work (Ssp1)
GST-GIV-NT-L249P (1-440)	pLIC GST	CCDC88a	Generated for this work (Ssp1)
His-GIV-NT-WT (1-440)	pLIC His	CCDC88a	Generated for this work (Ssp1)
His-GIV-NT-S245A; (1-440)	pLIC His	CCDC88a	Generated for this work (Ssp1)
His-GIV-NT-L249P; (1-440)	pLIC His	CCDC88a	Generated for this work (Ssp1)
Myc-AMPK-α2 WT	pcDNA 3.1	PRKAA2	Generated for this work
HA-K-Ras G12V	pcDNA 3.1	KRAS	Aznar et al., eLife 2015

RESULTS

AMPK binds and phosphorylates GIV at residue S245

A prior study that attempted to map human protein-protein interactions on a large scale by Mass Spectrometry (Ewing *et al.*, 2007) had identified GIV as a binding partner of the β-subunit of AMPK. Numerous studies have also demonstrated that AMPK binds and phosphorylates its substrates on a Serine or Threonine residue within the consensus sequence FxR/KxxS/TxxxL (Banko *et al.*, 2011; Marin *et al.*, 2015). We found such a consensus site within a short stretch of residues within the N-terminus of GIV (239-250 aa) that is evolutionarily conserved (**Figures 1A-C**). Using a previously solved crystal structure of CagA in complex with the AMPK family member MARK2, we generated a homology model of GIV bound to AMPK and found that the residues within the short stretch of GIV sequence and those at the flanks are compatible with GIV's ability to bind and get phosphorylated at Ser 245 (S245) by AMPKα.

To determine if GIV binds AMPKα, we carried out co-immunoprecipitation (co-IP) assays on Cos7 cells expressing myc-tagged AMPKα and analyzed AMPK-bound immune complexes for GIV (**Figure 1D**). These studies confirmed that full length endogenous GIV binds AMPKα in cells. GST-pulldown assays further confirmed that the N-terminal 440 aa of GIV are sufficient for binding AMPK (**Figure 1E**). These findings indicate that GIV binds AMPKα via its N-terminus, as expected based on the location of the aforementioned consensus motif/sequence.

Next, we performed in-vitro kinase assays using recombinant AMPK heterotrimers and bacterially expressed N-terminal fragments of GIV. AMPK phosphorylated GST-GIV WT (1-440 aa) but not the non-phosphorylatable mutant GST-GIV S245A (1-440 aa)

(**Figure 1F**), thereby validating the prediction based on homology modeling (**Figure 1A**). No phosphorylation was seen when GST-GIV 440-747 aa was used as substrate (**Figure 1F**), indicating that the phosphorylation we observe on GIV is specific and that AMPK uniquely targets exclusively the N-terminally located residue, S245. Taken together, these results demonstrate that GIV is a substrate of AMPK, and that S245 of GIV is the specific substrate site for the kinase in vitro.

We also noted that S245 of GIV is phosphorylated in cells, as reported in a previous high-throughput study to map the phosphoproteome of cancer cells (Zhou *et al.* 2013). To confirm if AMPK phosphorylates GIV at S245 in cells we generated a rabbit polyclonal antibody against phospho-Serine 245 (pS245) and carried out in vivo phosphorylation assays in cells coexpressing GIV-FLAG and myc-AMPK. Because AMPK has been largely described as a sensor of cellular energy (Hardie, 2011; Mihaylova & Shaw, 2011) and is activated in metabolic stress conditions, we triggered activation of AMPK by glucose starvation. We found that GIV was indeed phosphorylated in cells at S245 (**Figure 1G**). Taken together, these data indicate that GIV is phosphorylated on S245 in cells subjected to metabolic stress.

GIV phosphorylated at S245 localizes to cell-cell junctions

Both GIV and AMPK have been implicated in the maintenance of epithelial cell polarity and integrity of cell-cell junctions (Sasaki *et al*., 2015; Zheng & Cantley, 2007). To determine when and where the AMPK-GIV axis is activated in epithelial cells, we chose to study the localization of pS245 GIV by immunofluorescence in Type II Madin-Darby canine kidney (MDCK) cells, which are widely accepted as an ideal cell-based model system to study epithelial polarity, junctional integrity and epithelial morphogenesis. In

fact, prior work investigating either the role of GIV (Sasaki *et al*., 2015) or AMPK (Zheng & Cantley, 2007) in the context of cell polarity and in the maintenance of cell-cell junctions has extensively used the MDCK cells as the central model system. We found that AMPK-phosphorylated pS245 GIV localized to the plasma membrane (PM) in MDCK cells at the sites of cell-cell contact (**Figure 2**), whereas no PM-staining is seen in isolated single cells without contact. Localization of pS245 GIV at cell-cell contact sites was lost when cells reached full confluency and formed mature junctions when they domed, which represent the ultimate phase of epithelial polarization. As a positive control, these cells were also immunostained for occludin, a marker of tight junctions (**Figure 2**). When fully polarized domed MDCK monolayers were subjected to either energetic stress by glucose deprivation (No Glucose) or by exposure to low calcium states by treatment with EGTA, pS245 GIV was once again seen at the PM. RGB profile analyses confirmed that pS245 GIV and occludin colocalized at these sites, indicating that pS245 GIV localized to cell-cell junctions. As for the timing of when GIV and pS245 GIV localize to cell-cell junctions, we found that both localization and phosphorylation of GIV coincided with disruption of TJs (as marked by ZO-1; **Figure 3**). Furthermore, using cross-sections of Z-stacked images of MDCK cells treated with 4mM EGTA, we confirmed that pS245 GIV colocalizes with Occludin, a marker of tight junctions (TJs), but not β-Catenin, a marker of adherens junctions (AJs) (**Figure 4**). Taken together, these data demonstrate that pS245 GIV is primarily located in the cell-cell contact sites, more specifically, at the TJs; such localization reaches prominence during conditions that require the formation of new junctions (e.g., monolayers of cells coming into contact, or domed cells exposed to EGTA or energetic stress conditions that disrupt cell-cell junctions). These findings suggest that

the AMPK-GIV axis, of which pS245 GIV is a product, may play a role in the formation of cell-cell junctions and polarization in immature epithelial cells, and be involved in the maintenance of junctions in mature cells exposed to conditions that destabilize junctions. Little or no pS245GIV was observed at cell-cell contact sites in domed monolayers at steady-state, which may indicate two possibilities: 1) pS245 GIV may not be needed in the maintenance of junctions at steady-state, or 2) pS245 GIV may be required for the maintenance of TJs, but is rapidly dephosphorylated (it may have a short half-life), thereby preventing its accumulation and consequently, impairing its detection at that site.

Phosphorylation of GIV at S245 by AMPK is essential for junctional integrity

To investigate the role of phosphorylation of GIV at S245 in the epithelia, we generated MDCK cell lines stably expressing wild-type (WT) FLAG-tagged GIV (GIV-FLAG) or GIV-FLAG S245A (SA; non-phosphorylatable mutant resembling a constitutively dephosphorylated state), or GIV-FLAG S245D (SD; phosphomimetic mutant resembling a constitutively phosphorylated state) (**Figure 5A**). Immunofluorescence studies confirmed that each cell line expressing GIV-FLAG was indistinguishable from the others at steady-state, in that they all grew into confluent monolayers comprised of completely polarized cells, without any obvious defect in the localization of E-Cadherin, Occludin, ZO-1 or β-Catenin (data not shown). However, distinct phenotypes were observed when these cells were exposed either to energetic stress by glucose deprivation (**Figure 5B**) or to low calcium states in the presence of EGTA (**Figure 6**). Under these conditions that trigger the disassembly of cell-cell junctions, MDCK cells expressing the non-phosphorylatable GIV-SA mutant were more susceptible compared to control MDCK parental cells or cells expressing GIV-WT, as determined by

the premature loss of TJ proteins ZO-1 and occludin from cell-cell junctions (**Figure 5, 6**). By contrast, the MDCK cells expressing the phosphomimetic GIV-SD mutant were more resistant compared to cells expressing GIV-WT (**Figure 5, 6**), as determined by the persistence of TJ proteins, ZO-1 and occludin at cell-cell junctions for prolonged periods of time. Additionally, GIV SA cells exhibited increased actin remodeling compared to WT and SD cells, indicative of junctional instability, loss of polarity and cell-flattening. These findings indicate that phosphorylation of GIV at S245 is required for junctional stability after energetic stress.

Prior studies have shown that inhibition of AMPK (either by depletion, or chemical inhibition or by expression of dominant negative kinase) makes TJs vulnerable to disruption and have concluded that kinase activity of AMPK is required for the functional integrity of TJs. We asked if phosphorylation of GIV at S245 by AMPK may serve as a key link between the kinase and its role in stabilization of TJs. To investigate if such is the case, MDCK cell lines were treated with Compound C, a known AMPK inhibitor for increasing time periods and observed for disruption of cell-cell junctions (**Figure 7A and B**). We found that MDCK-GIV-SD cells were virtually insensitive to the action of Compound C compared to parental and MDCK-GIV-WT control cells, indicating that phosphorylation of GIV at S245 is largely sufficient to maintain TJs which is able to bypass or rescue the effect of AMPK inhibition by Compound C. By contrast, MDCK-GIV-SA cells were highly susceptible to the action of Compound C, showing widespread loss of cell-cell junctions. These findings indicate that phosphorylation of GIV at S245 is essential for the preservation of TJ integrity in the setting of energetic stress and that GIV is a major

substrate and effector via which AMPK increases junctional stability and epithelial polarity in the setting of energetic stress.

Because TJs regulate the paracellular permeability and are crucial for the integrity of the epithelial barrier, next we measured paracellular ion permeability to evaluate the functional integrity of TJs by assessing transepithelial electrical resistance (TEER) across the various MDCK cell lines stably expressing GIV WT and mutants (**Figure 8**). Consistent with our findings by immunofluorescence (**Figure 6**), the drop in TEER was less in MDCK-GIV-SD cells compared to MDCK-GIV-WT (25% compared to 50%; **Figure 8**), indicating that phosphorylation of GIV at S245 stabilizes TJs and makes epithelial monolayers resistant to the action of EGTA. Conversely, during the recovery phase after washout of EGTA, MDCK-GIV-WT cells increased TEER by ~2-fold within 4 h, whereas MDCK-GIV-SA cells regained ~1.5 fold resistance within the same time period (**Figure 8**). These findings indicate that phosphorylation of GIV at S245 is required for stabilizing junctional integrity during disassembly as well as for regaining junctional integrity during assembly. These findings also suggest that AMPK-dependent GIV phosphorylation stabilizes epithelial cell membrane barrier function, particularly during periods of junctional stress and recovery.

Phosphorylation of GIV at S245 by AMPK regulates epithelial morphogenesis

To determine if phosphorylation of GIV at S245 regulates epithelial morphogenesis, we carried out 3D cyst formation assays using MDCK cells, which is a stringent assay that allows for the determination of whether the 3D culture is fully polarized. When cultivated in a 3D collagen matrix, MDCK cells form cysts, which are spherical structures containing a single lumen in the middle and apical-basal polarity in the

surrounding cells (O'Brien, Zegers, & Mostov, 2002). Cells with disrupted polarity may form abnormal cysts with multiple lumens, elongated structures, and larger size. We found that MDCK-parental and MDCK-GIV-WT cells cultivated in a 3D collagen matrix formed similarly intermediate sized cysts each containing a single lumen, with infrequent occurrence of tubular structures (**Figure 9**). MDCK-GIV-SD cells consistently formed smaller cysts with single lumens, but no tubular structures. By contrast, MDCK-GIV-SA cells formed multiple-lumen cysts and an abundance of tubular structures (**Figure 9**). These data indicate that phosphorylation on GIV S245 is a key determinant of cell polarity and epithelial morphogenesis-- phosphorylation favors polarized normal growth, whereas absence of phosphorylation favors tubule formation, branching and a multi-lumen phenotype.

Deregulation of the AMPK-GIV axis in cancer cells trigger anchorage-independent growth

Loss of cell polarity is commonly associated with tumor development and cancer progression. Because phosphorylation of GIV at S245 by AMPK regulates TJ formation and stability, we wondered if AMPK-dependent phosphorylation and signaling via GIV is impaired during tumorigenesis. First, bioinformatic analysis performed by using the Catalogue of Somatic Mutations in Cancer (COSMIC) database revealed the presence of a GIV L249P mutation localized 4 sites downstream of residue S245, found in a patient with colorectal cancer. The L249 residue is within the consensus sequence (FxR/KxxS/Txxx**L**) recognized by AMPK to bind and phosphorylate its substrates. Homology modeling provided valuable clues into what might be the consequence of a substitution of L249 with P (**Figure 10A**). We noted that the residue L249 makes a large contribution to the binding

energy due to the fact that it is buried in a hydrophobic pocket on AMPK. Second, this model also showed that the amide hydrogen of the residue L249 makes a hydrogen bond with the S184 on AMPK which is lost once it is mutated to Proline, inducing steric clash (**Figure 10A**). Together, these predictions indicate that the L249P mutation (henceforth, LP) may disrupt the interaction between GIV and AMPK, and therefore prevent phosphorylation of S245. Both in vitro (**Figure 10B**) and in cellulo (**Figure 10C**) kinase assays confirmed these predictions; we found that AMPK is able to phosphorylate GST-GIV WT to a much greater extent than both the non-phosphorylatable mutant GST-GIV SA and the GST-GIV LP (**Figure 10B**). Similarly, glucose starvation triggered the phosphorylation of GIV-WT, but not GIV-LP in Cos7 cells (**Figure 10C**).

Next we asked if the LP mutation can affect epithelial membrane barrier function during recovery after EGTA. Much like what was observed in MDCK-GIV-SA cells, cells expressing GIV-LP showed significant impairment in recovery of TEER during recovery after EGTA treatment compared to MDCK-GIV-WT (**Figure 10D**). We then tested the LP mutant in cyst growth assays, and found that it exhibited similar characteristics to the SA mutant, including larger sized, multi-lumen cysts and an abundance of multi-lumen tubules (**Figure 10E**). Together, these results indicate that the cells expressing GIV-LP mutant share the same phenotypes as the MDCK-GIV-SA cells. Because GIV-LP cannot be phosphorylated at S245 by AMPK, findings also suggest impairment of phosphorylation and a loss of tight junction stabilizing effects of such phosphorylation as the common basis for dysregulated epithelial tissue structure and function.

Junctional stability and epithelial cell polarity is a key deterrent of tumor initiation. Upon loss of junctional stability and apical-basal polarity, epithelial cells can undergo

excess proliferation and neoplasia, which may eventually result in tumor growth and progression. Additionally, loss of cell polarity contributes to epithelial mesenchymal transition (EMT), which results in anchorage independent cell growth and increased motility. Therefore, factors that work to maintain polarity can be viewed as non-canonical tumor suppressors (Lee & Vasioukhin, 2008). Up to this point, our experiments have shown that GIV pS245 acts to stabilize epithelial cell polarity both during normal polarization and stress responses. Therefore, we were curious to discover the role of S245 phosphorylation in tumor progression. An anchorage independent 3D tumor growth assay and anchorage dependent 2D colony formation assay were designed using cells from the DLD1 human colorectal adenocarcinoma cell line. DLD1 cells stably expressing full length GIV-flag WT, S245A, S245D, or L249P were either grown in an agarose gel matrix for the 3D assay or a flat-bottom well for the 2D assay. Additionally, an NIH3T3 transformation assay was performed to observe the effects of S245 mutations on K-Ras G12V transformed cells. We observed that SD tumors exhibited the smallest growth, while SA and LP tumors grew the most in both the DLD1 and NIH3T3 3D growth assays (**Figure 10F, 10G, 10J**). In the 2D growth assay, these results were reversed; SD cells grew the most colonies while SA and LP cells grew the least (**Figure 10H and 10I**). These results indicate that phosphorylation of GIV at S245 may indeed have a tumor suppressive role via its polarity stabilizing functions and could restrict growth to anchorage-dependent conditions, but trigger anoikis when anchorage is lost.

The Results section is currently being prepared for submission for publication. Dr. Pradipta Ghosh and Dr. Nicolas Aznar have served as co-authors; the thesis author was the

primary investigator and author of this material. Dr. Aznar has contributed data to Figures 1, 3, 5, 6, 7, 9, and 10.

Figure 1. AMPK binds and phosphorylates GIV at S245. (A) Homology model of GIV-bound AMPKα generated using the structure of constitutively active Par1-MARK2 (a member of the AMPK family of kinase) in complex with the CagA protein encoded by pathologic strains of Helicobacter pylori (Nesic et al 2010; PDB: 3IEC). (B) Consensus phosphorylation site for previously identified substrates of AMPK is aligned with the putative AMPK substrate site in human GIV. Conserved residues are highlighted with colors. (C) The sequence encompassing the putative AMPK substrate motif was aligned among various species using ClustalW. Conserved residues are shaded in black and similar residues in gray. Conserved residues that preserve the consensus sequence are highlighted in blue. The predicted phosphorylation site (S245) is highlighted in yellow. (D) Immunoprecipitations were carried out on lysates of Cos7 cells expressing myc-AMPKα using anti-myc mAb. Immune complexes were analyzed for endogenous GIV and myc (AMPKα). (E) Lysates of Cos7 cells expressing myc-AMPKα was used as source of AMPK in pulldown assays with GST or GST-GIV (aa 1-440) immobilized on glutathione beads. Bound proteins were analyzed for myc (AMPKα), Gαi3 (negative control; because G protein binds GIV's C-terminus, not N-terminus) and endogenous GIV (positive control; because GIV homo-oligomerizes via its NT). (F) In vitro kinase assays were carried out using recombinant AMPK heterotrimers (α/β/γ) and bacterially expressed and purified GST-GIV proteins or GST alone (negative control) and γ -32P [ATP]. Phosphoproteins were analyzed by SDS PAGE followed by autoradiography. (G) In cellulo kinase assay was carried out by co-expressing FLAG tagged GIV-WT and myc-AMPKα, and stimulating AMPK by glucose depravation for 6 h prior to lysis. GIV was immunoprecipitated from these lysates and analyzed for total GIV (tGIV) and pS245 GIV by immunoblotting.

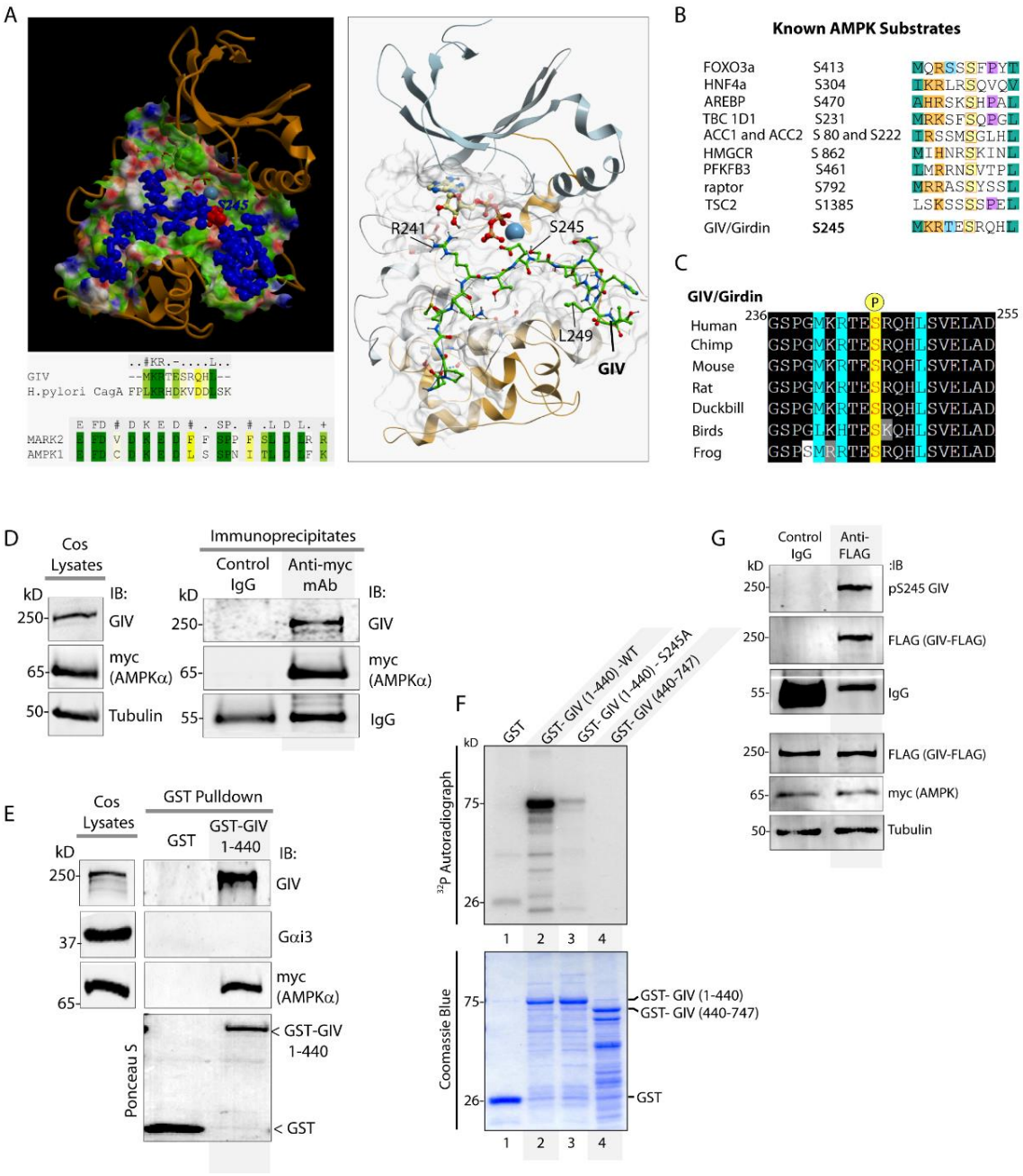
A
S245
R241
S245
L249
GIV
B
Known AMPK Substrates
FOXO3a S413
HNF4a S304
AREBP S470
TBC 1D1 S231
ACC1 and ACC2 S 80 and S222
HMGCR S 862
PFKFB3 S461
raptor S792
TSC2 S1385
GIV/Girdin S245
C
GIV/Girdin
P
Human
Chimp
Mouse
Rat
Duckbill
Birds
Frog
D
Cos Lysates
Immunoprecipitates
Control IgG
Anti-myc mAb
kD
IB:
GIV
myc (AMPKα)
Tubulin
IgG
E
Cos Lysates
GST Pulldown
GST
GST-GIV 1-440
Gαi3
Ponceau S
F
GST
GST- GIV (1-440) -WT
GST- GIV (1-440) - S245A
GST- GIV (440-747)
32P Autoradiograph
Coomassie Blue
G
Control IgG
Anti-FLAG
pS245 GIV
FLAG (GIV-FLAG)
IgG
myc (AMPK)
Tubulin

Figure 2. S245-phosphorylated GIV localizes to cell-cell junctions. MDCK cells growing on glass cover slips were treated as indicated, fixed, stained for occludin (green), pS245 GIV (red) and DAPI (blue; nuclei) and analyzed by confocal microscopy at various stages during their growth into confluent monolayers. RGB plots on the right assess the degree of colocalization between pS245GIV and occludin along the lines in the corresponding images.

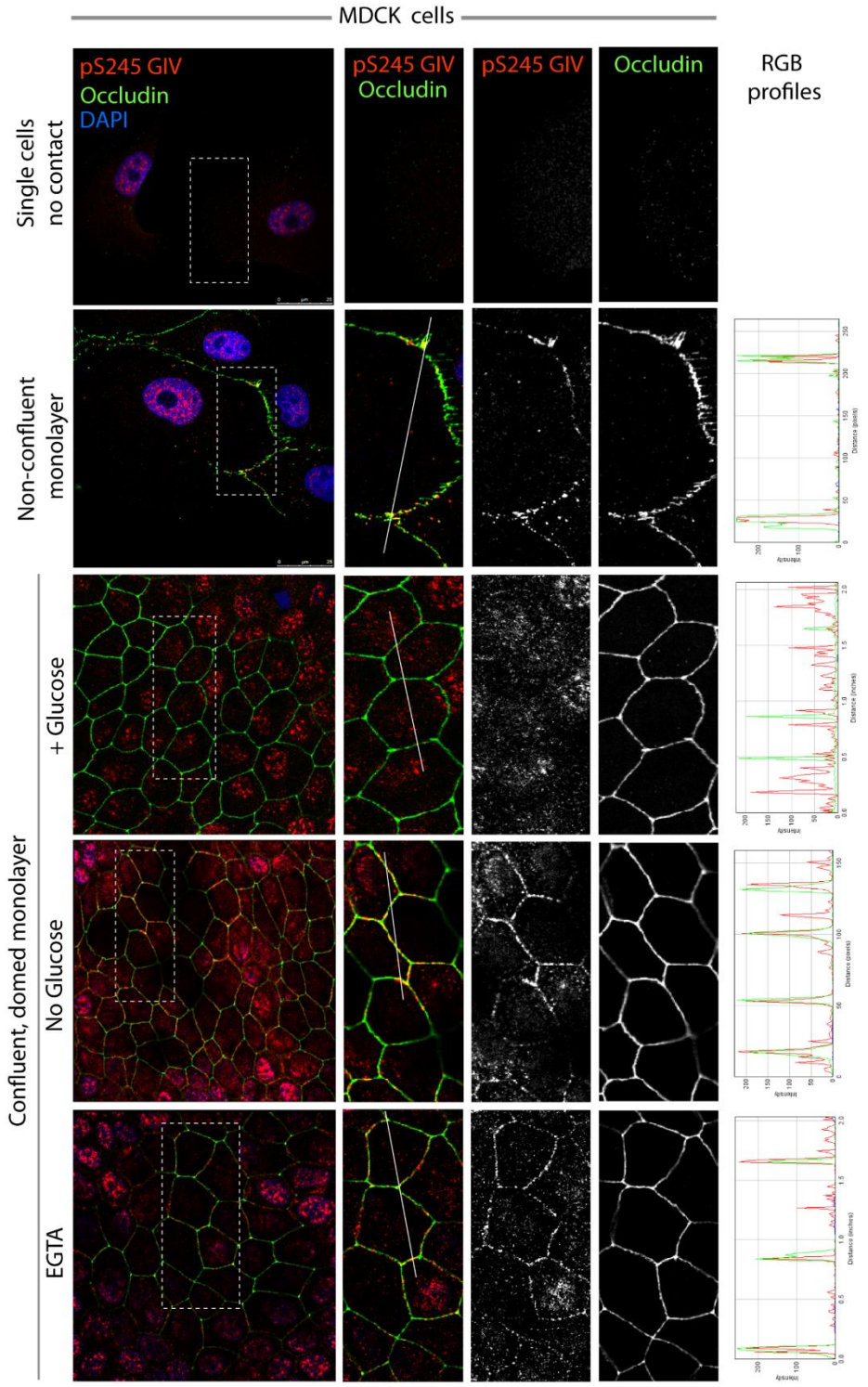
MDCK cells
pS245 GIV
Occludin
DAPI
pS245 GIV
Occludin
pS245 GIV
Occludin
RGB profiles
Single cells no contact
Non-confluent monolayer
Confluent, domed monolayer
+ Glucose
No Glucose
EGTA

Figure 3. GIV localizes to and is phosphorylated at cell-cell junctions in response to energetic stress. MDCK cells were grown to full confluency into domed monolayers prior to subjecting them to energetic stress by exposing to low glucose media for indicated periods of time. Cells were subsequently fixed, stained for total (tGIV), pS245 GIV, or co-stained for ZO-1 (a TJ marker) and β Catenin (an AJ marker). GIV localizes to cell-cell contact sites (arrowheads), most prominently at 120 min after glucose starvation, which coincides also with prominence of pS245 GIV at similar cell-cell contact sites. At 120 min, the localization of the TJ-marker, ZO-1 is reduced at cell-cell contact sites, whereas the localization of β Catenin remains unchanged.

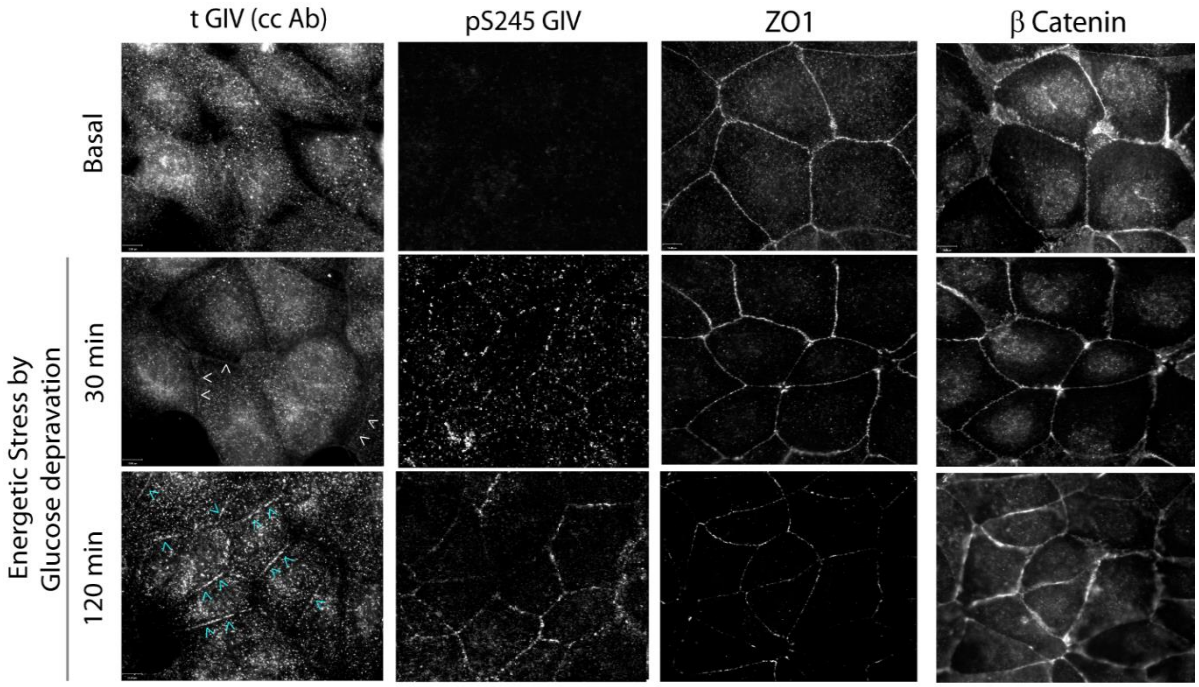
t GIV (cc Ab)
pS245 GIV
ZO1
β Catenin
Basal
30 min
120 min
Energetic Stress by
Glucose depravation

Figure 4. S245-phosphorylated GIV localizes to tight junctions. MDCK cells were grown to full confluency into domed monolayers prior to exposing them to low calcium containing media for 6 h (i.e., by addition of EGTA) prior to fixation. Fixed cells were costained for pS245 GIV (red) and either the TJ-marker occludin (Left; green) or the AJ-marker β Catenin (Right; green) and analyzed by analyzed by confocal microscopy (z-stack projections and x-z cross-sections. Top: Representative confocal images are shown, each taken at the level of TJs (marked by occludin; left) and AJs (marked by β Catenin; right). Middle: RGB profiles showed that pS245 GIV colocalized with occludin but not β Catenin. Bottom: Sections through the 3D reconstruction of a confocal Z-stack confirms that the pS245 GIV colocalizes with TJ marker occludin, and lies just apical to the AJ marker β Catenin. Schematic summarizes the localization of pS245 GIV and its relationship to TJ and AJs.

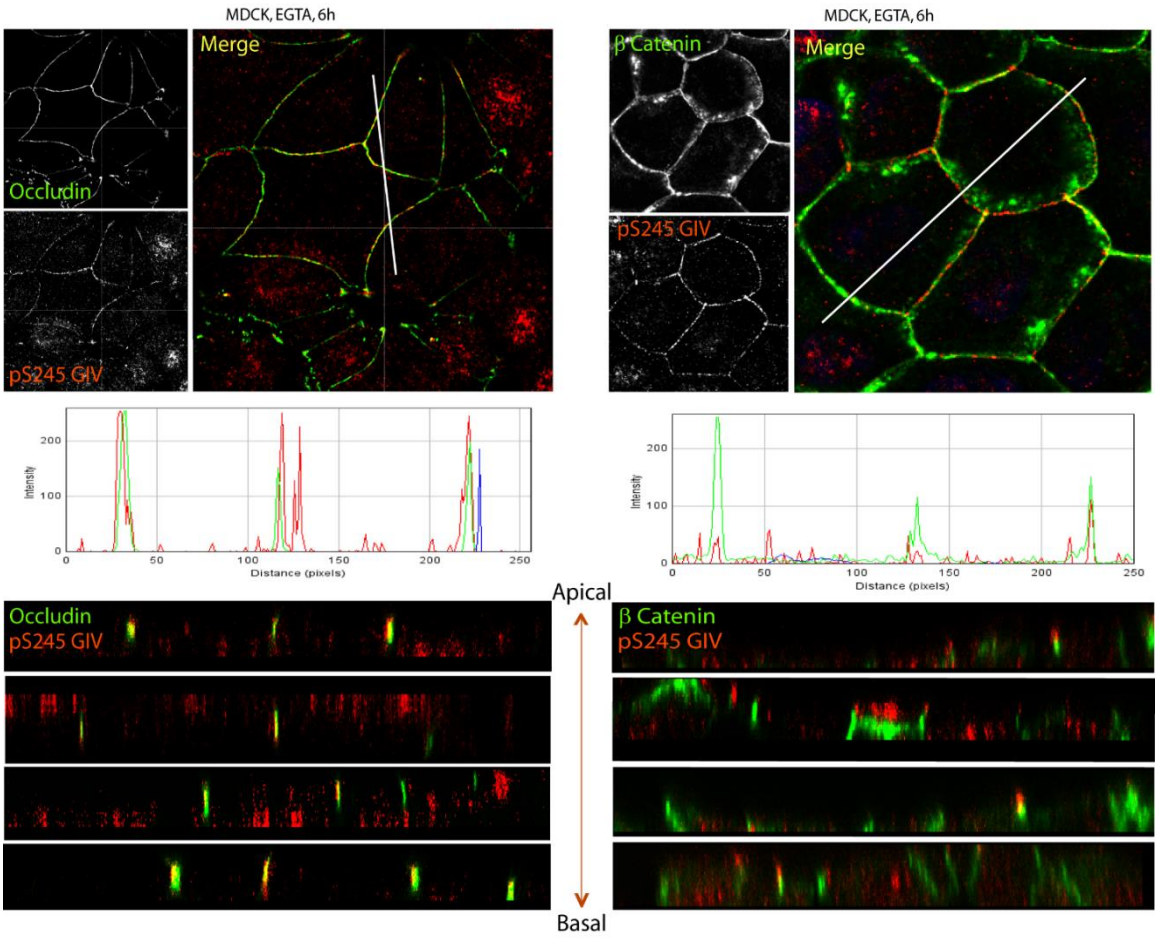
MDCK, EGTA, 6h
Occludin
Merge
pS245 GIV
MDCK, EGTA, 6h
β Catenin
Merge
pS245 GIV
Intensity
Distance (pixels)
Apical
Occludin
pS245 GIV
β Catenin
pS245 GIV
Basal

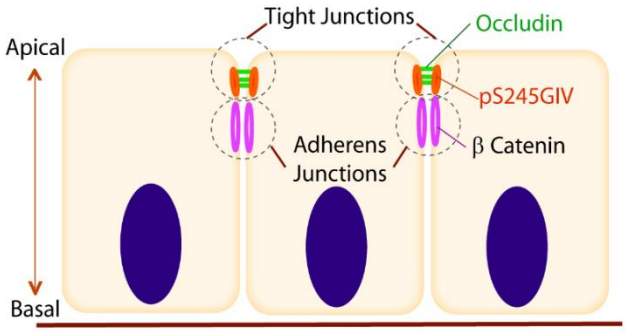
Tight Junctions
Occludin
Apical
pS245GIV
Adherens
Junctions
β Catenin
Basal

Figure 5. Phosphorylation of GIV at S245 stabilizes tight junctions during energetic stress. (A) Whole cell lysates of MDCK cells stably expressing GIV-WT or various mutants were analyzed for GIV and tubulin by immunoblotting. (B) MDCK cell lines stably expressing various GIV constructs were grown to full confluency into domed monolayers prior to subjecting them to energetic stress by exposing to low glucose media for 30 min prior to fixation. Fixed cells were stained for Phalloidin (actin), E cadherin, ZO-1 or β Catenin and analyzed by confocal microscopy.

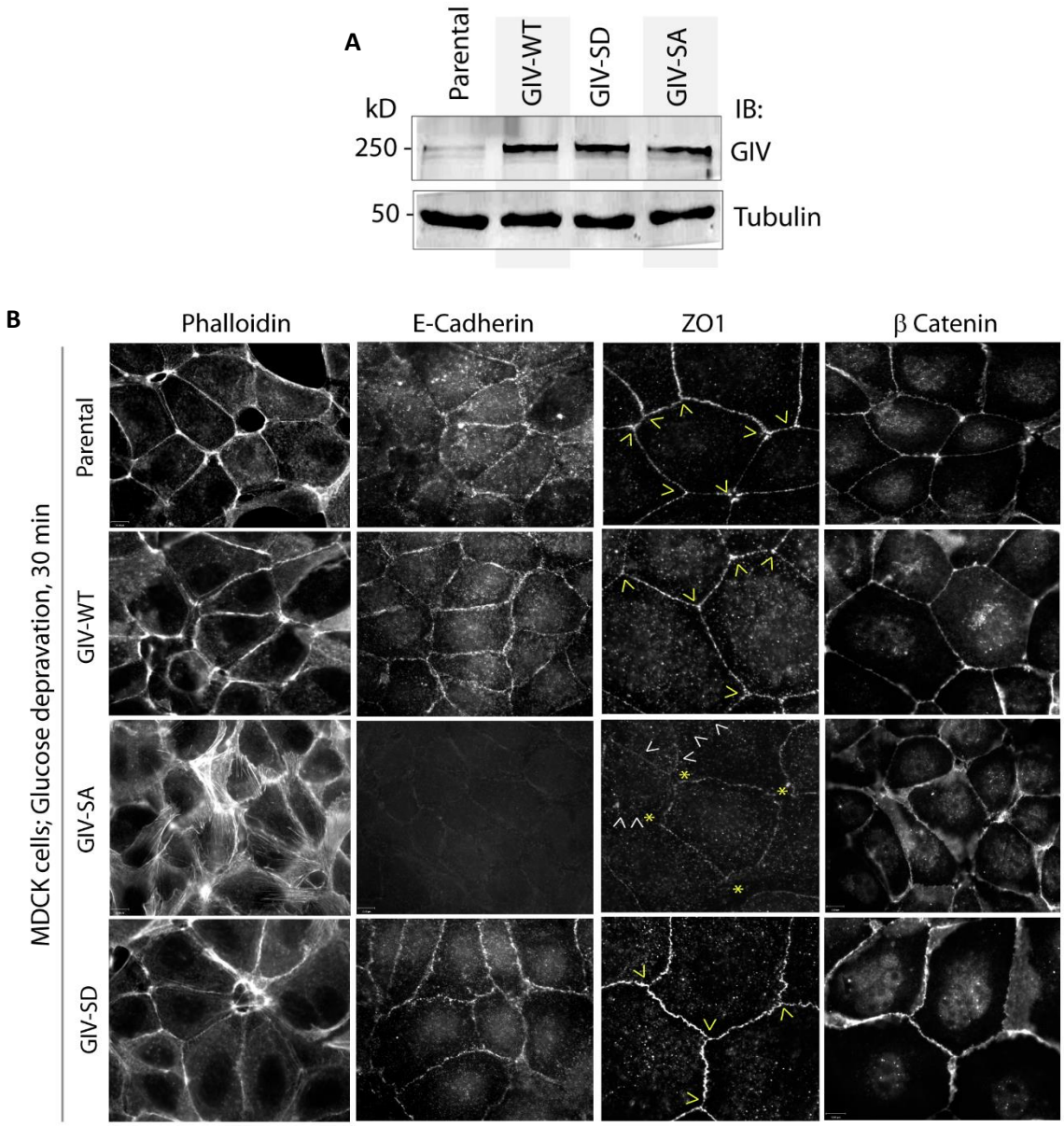
A
Parental
GIV-WT
GIV-SD
GIV-SA
kD
IB:
250
GIV
50
Tubulin
B
Phalloidin
E-Cadherin
ZO1
β Catenin
MDCK cells; Glucose depravation, 30 min
Parental
GIV-WT
GIV-SA
GIV-SD

Figure 6. Phosphorylation of GIV at S245 stabilizes tight junctions under low calcium states. Parental MDCK cells and MDCK cell lines stably expressing various GIV constructs were grown to full confluency into domed monolayers prior to subjecting them to low calcium media by exposure to EGTA for the indicated periods of time prior to fixation. Fixed cells were stained for occludin, ZO-1 and DAPI (nuclei; blue) and analyzed by confocal microscopy.

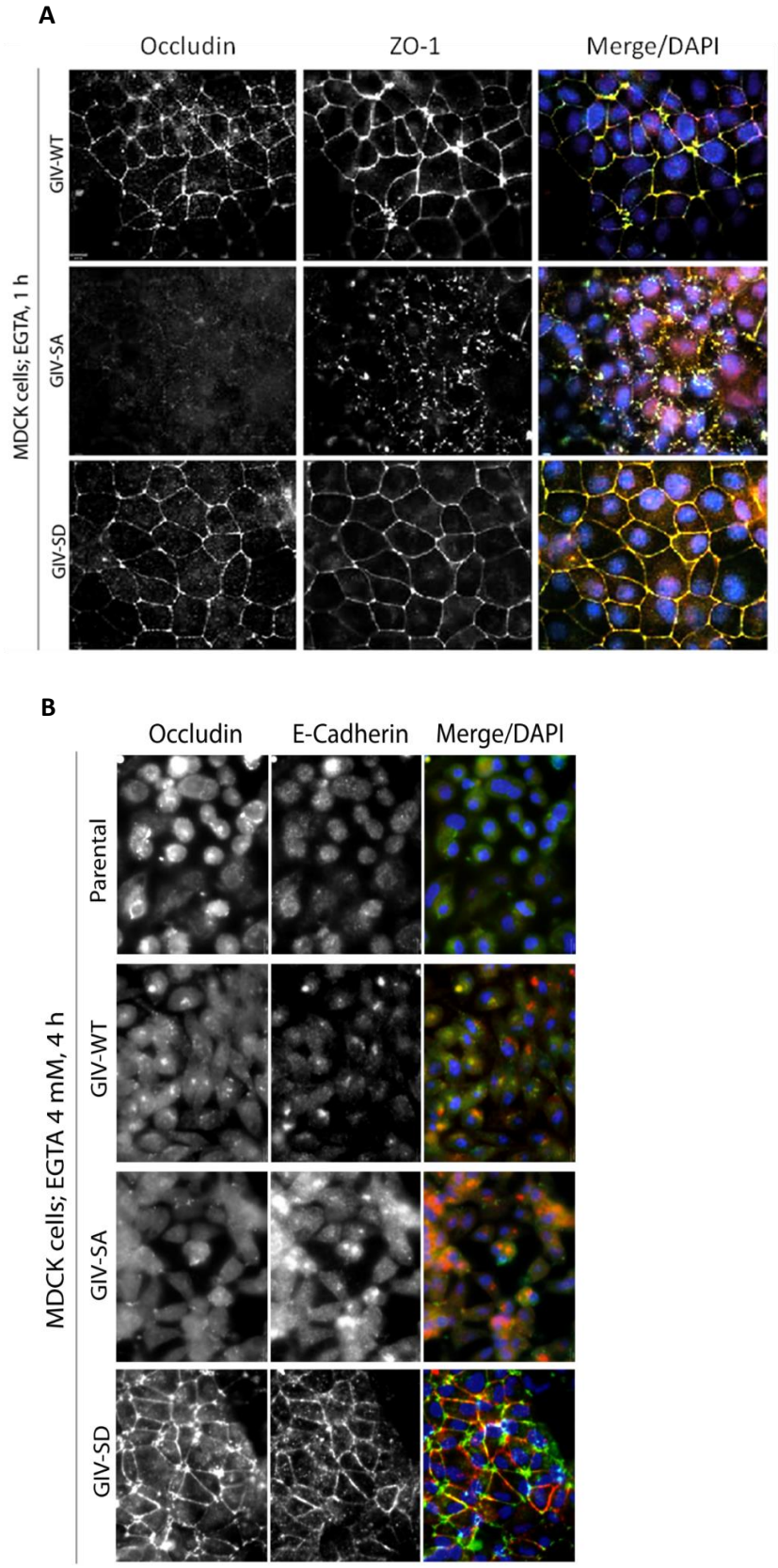
A
Occludin
ZO-1
Merge/DAPI
MDCK cells; EGTA, 1 h
GIV-WT
GIV-SA
GIV-SD
B
Occludin
E-Cadherin
Merge/DAPI
MDCK cells; EGTA 4 mM, 4 h
Parental
GIV-WT
GIV-SA
GIV-SD

Figure 7. Phosphorylation of GIV at S245 stabilizes tight junctions during chemical inhibition of AMPK by Compound C. (A) MDCK cell lines stably expressing various GIV constructs were grown to full confluency into domed monolayers prior to exposing them to Compound C for 20 h and the monolayers were analyzed by light microsocpy. Unlike the monolayers of MDCK-GIV-WT and SA cells, the MDCK-GIV-SD cells were insensitive to the effects of Compound C. (B) MDCK cell lines stably expressing various GIV constructs were grown to full confluency into domed monolayers prior to exposing them to Compound C for indicated periods of time prior to fixation. Fixed cells were stained for occludin (green) and DAPI (blue; nuclei) and analyzed by confocal microscopy.

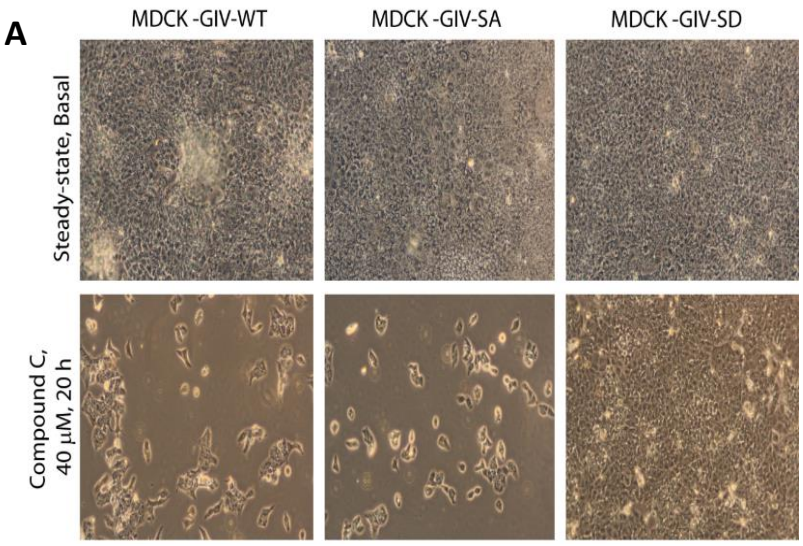
A
MDCK -GIV-WT
MDCK -GIV-SA
MDCK -GIV-SD
Steady-state, Basal
Compound C, 40 μM, 20 h

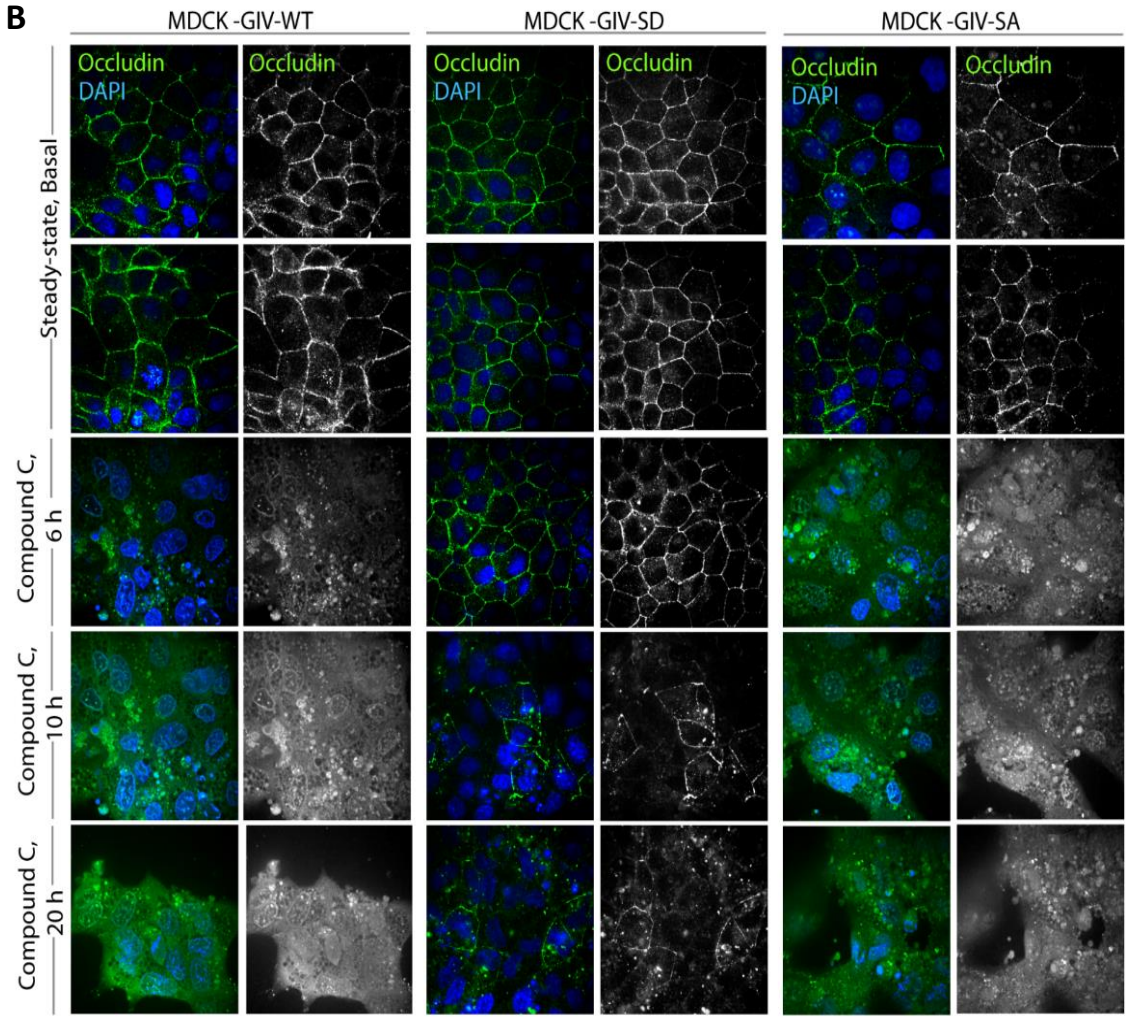
B
MDCK -GIV-WT
MDCK -GIV-SD
MDCK -GIV-SA
Occludin
DAPI
Occludin
Steady-state, Basal
Compound C, 6 h
Compound C, 10 h
Compound C, 20 h

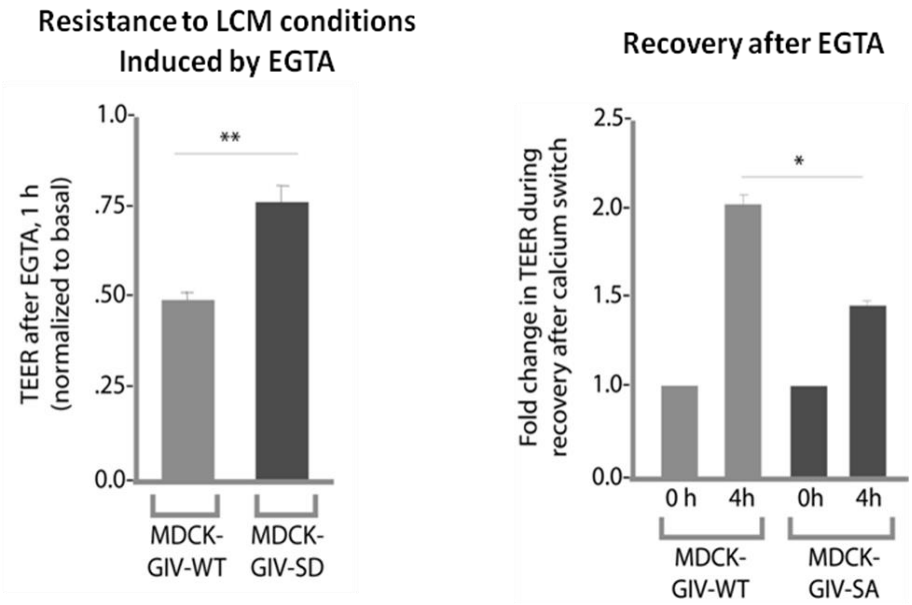

Figure 8. Phosphorylation of GIV at S245 is essential for epithelial barrier functions. Changes in transepithelial electrical resistance (TEER) was measured across monolayers of MDCK cells expressing the indicated GIV construct either during exposure to low calcium media induced by the addition of EGTA (LCM; left) or during recovery from EGTA (right). While MDCK-GIV-SD cells preserve TEER better than control (MDCK-GIV-WT) cells during EGTA exposure, MDCK-GIV-SA cells show impairment in regaining TEER during recovery after EGTA.

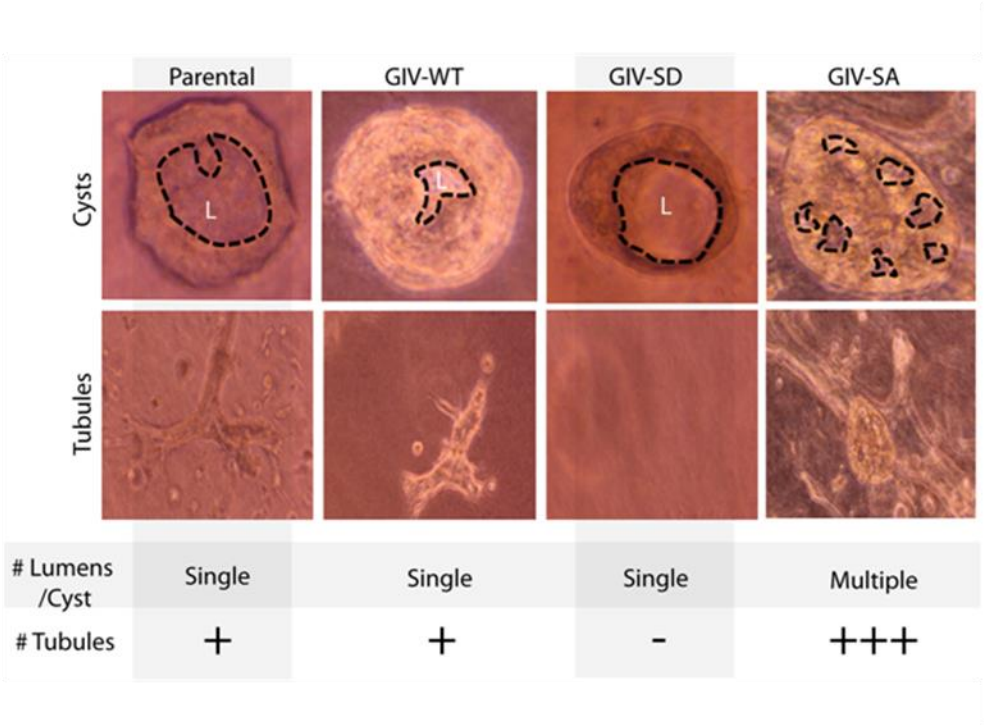

Figure 9. Phosphorylation of GIV at S245 is essential for epithelial morphogenesis. Parental MDCK cells and MDCK cell lines stably expressing various GIV constructs were grown in 3D cultures embedded in collagen containing matrix for 2 weeks and analyzed for the formation of cyst and tubular structures by light microscopy. Representative cysts and tubular structures are shown. L = lumen. Images were captured at 20 X magnification.

Figure 10. An oncogenic GIV mutant that impairs phosphorylation of GIV at S245 reduces junctional stability and augments anchorage-independent growth. (A) Homology model of GIV-bound AMPKα is shown on the left. Boxed area in the model is magnified to show the impact of replacing Leu (L) at 249 with Pro (P). While L249 is predicted to be favorably buried in a hydrophobic pocket in AMPKα, contributing to binding energy, P249 is expected to induce a steric clash. (B) In vitro kinase assays were carried out using recombinant AMPK heterotrimers (α/β/γ) and bacterially expressed and purified His-GIV (WT and mutants) and His-Gαi3 (negative control) and γ -32P [ATP]. Phosphoproteins were analyzed by SDS PAGE followed by coomassie blue staining to visualize His-tagged proteins (left) and autoradiography to visualize phosphorylation (right). (C) Immunoprecipitation was carried out using either control IgG (lane 1) or anti-FLAG mAb (all other lanes) from lysates of Cos7 cells co-expressing myc-AMPKα and either GIV-WT or GIV-LP FLAG-tagged proteins that were subjected or not subjected to energetic stress by exposure to glucose depravation prior to lysis. Immune precipitates were analyzed for pS245 GIV and total GIV (FLAG) by immunoblotting. (D) Change in TEER was measured across monolayers of MDCK cells expressing the indicated GIV construct during recovery from low calcium growth conditions in the presence of EGTA. Compared to MDCK-GIV-WT cells, MDCK-GIV-LP cells show impairment in regaining TEER during recovery after EGTA. (E) Parental MDCK cells and MDCK cell lines stably expressing GIV-WT or GIV-LP constructs were grown in 3D cultures embedded in collagen containing matrix for 2 weeks and analyzed for the formation of cyst and tubular structures by light microscopy. Representative cysts and tubular structures are shown. L = lumen. Images were captured at 20 X magnification. (F-G) DLD1 colorectal cancer cells stably expressing various GIV constructs were analyzed for their ability to form colonies in soft agar for 2-3 weeks. In panel F, representative fields photographed at 20X magnification are shown. The number of colonies was counted by light microscopy throughout the depth of the matrix in 15 randomly chosen fields. In panel G, bar graphs display the number of colonies (Y axis) seen in each cell line in F. (H-I) DLD1 cells used in F were analyzed for their ability to form adherent colonies on plastic plates 1-2 weeks prior to fixation and staining with crystal violet. In panel H, a photograph of the crystal violet-stained 6-well plate is displayed. The number of colonies was counted by ImageJ (Colony counter). In panel I, bar graphs display the % inhibition of colony formation (Y axis) seen in each cell line in H normalized to control DLD1 cells. (J) NIH3T3 cells stably expressing HA-KRas G12V alone, or coexpressing HA-KRas G12V with GIV-WT-FLAG or various mutants were analyzed for their ability to form colonies in soft agar prior to staining with MTT. Bar graph shows the number of colonies formed / plate (Y axis) in each condition.

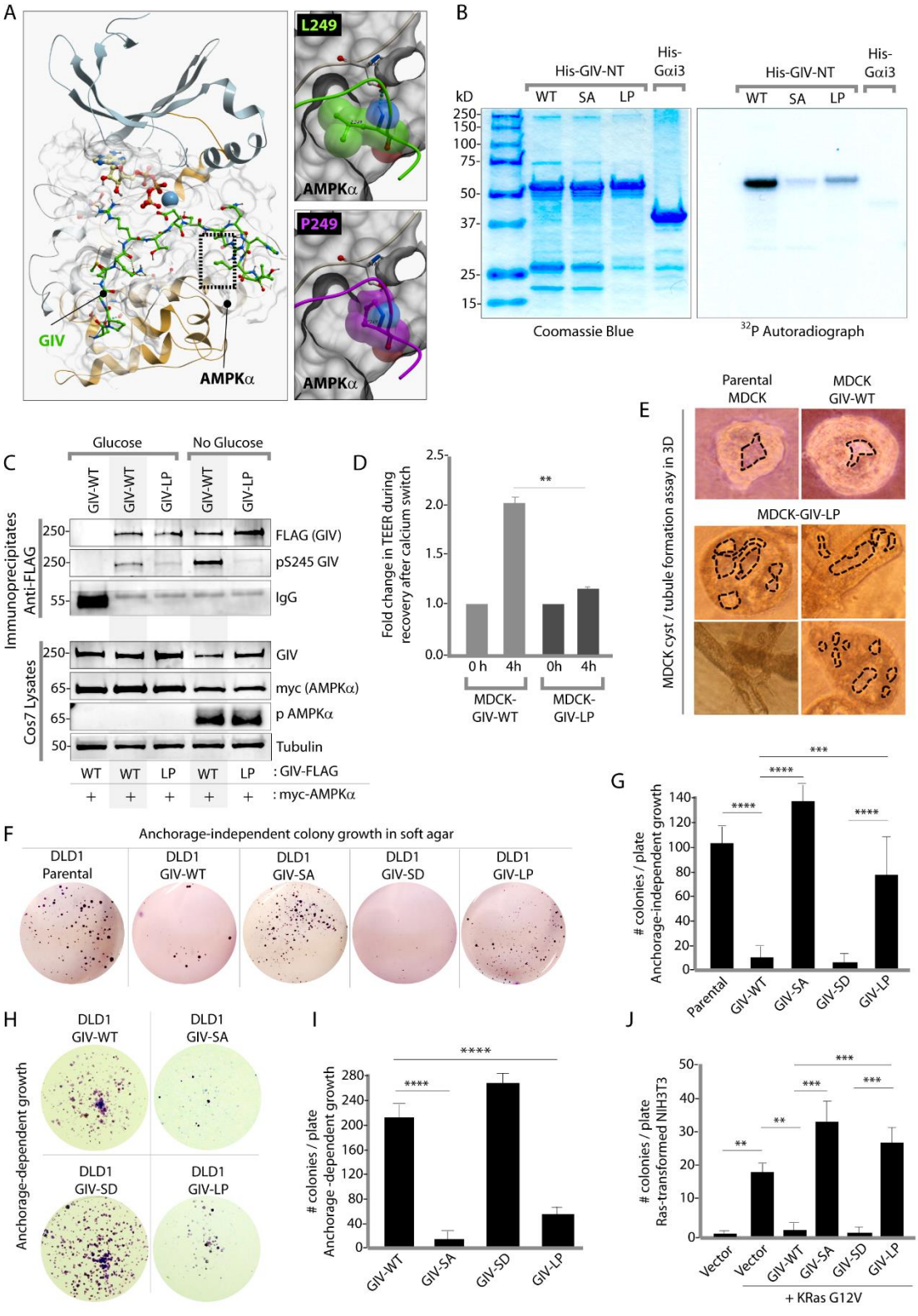
A
L249
AMPKα
P249
AMPKα
GIV
AMPKα
B
His-GIV-NT
His-Gαi3
WT SA LP
kD
250-
150-
100-
75-
50-
37-
25-
15-
Coomassie Blue
32P Autoradiograph
C
Glucose
No Glucose
GIV-WT GIV-WT GIV-LP GIV-WT GIV-LP
Immunoprecipitates Anti-FLAG
250-
250-
55-
FLAG (GIV)
pS245 GIV
IgG
Cos7 Lysates
250-
65-
65-
50-
GIV
myc (AMPKα)
p AMPKα
Tubulin
WT WT LP WT LP : GIV-FLAG
+ + + + + : myc-AMPKα
D
Fold change in TEER during recovery after calcium switch
2.5
2.0
1.5
1.0
0.0
**
0 h 4h 0h 4h
MDCK-GIV-WT
MDCK-GIV-LP
E
Parental MDCK
MDCK GIV-WT
MDCK-GIV-LP
MDCK cyst / tubule formation assay in 3D
F
Anchorage-independent colony growth in soft agar
DLD1 Parental
DLD1 GIV-WT
DLD1 GIV-SA
DLD1 GIV-SD
DLD1 GIV-LP
G
colonies / plate Anchorage-independent growth
140
120
100
80
60
40
20
0
***
****
****
****
Parental
GIV-WT
GIV-SA
GIV-SD
GIV-LP
H
DLD1 GIV-WT
DLD1 GIV-SA
DLD1 GIV-SD
DLD1 GIV-LP
Anchorage-dependent growth
I
colonies / plate Anchorage-dependent growth
280
240
200
160
120
80
40
0
****
****
GIV-WT
GIV-SA
GIV-SD
GIV-LP
J
colonies / plate Ras-transformed NIH3T3
50
40
30
20
10
0
***
***
***
**
**
Vector
Vector
GIV-WT
GIV-SA
GIV-SD
GIV-LP
+ KRas G12V

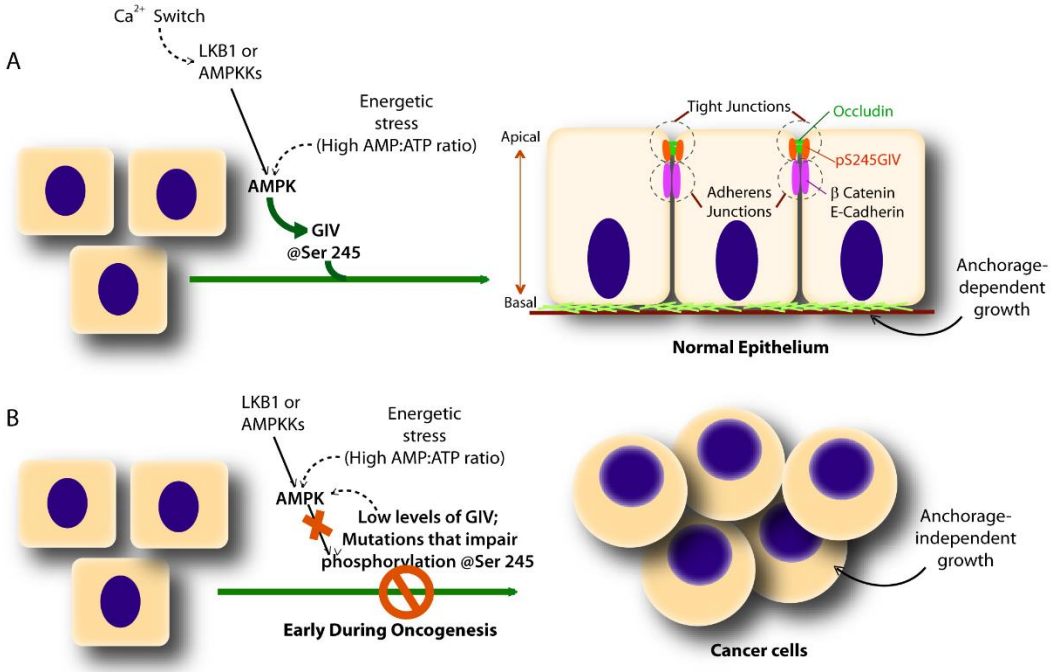

Figure 11. Overall working model summarizing how the AMPK-GIV axis impacts epithelial properties in the physiology and cancer. This schematic summarizes the key findings in this work, which is the identification of GIV as a substrate for AMPK. A variety of triggers, e.g., Calcium switch or activation of upstream LKB1 or other AMPKKs or energetic stress that depletes cellular ATP (that increase AMP:ATP ratio) converge on AMPK to activate this key metabolic sensor. AMPK is known to promote junctional stability and preserve or induce polarized cell growth. Evidence provided here indicates that GIV is a key downstream substrate and effector of AMPK, and that phosphorylation of GIV at S245 by AMPK in the normal epithelium (A) is necessary and sufficient to stabilize the tight junctions and maintain polarized cell growth in the setting of energetic stress. (B) In transformed tumor cells, phosphorylation of GIV at S245 by AMPK supports anchorage-dependent growth but inhibits anchorage-independent growth. Inhibition of this phospho-event, either due to low levels of GIV in tumor cells or due to mutation of key residues in GIV that impair such phosphorylation, allows tumor cells to become proficient in anchorage-independent growth, a hallmark of cancer.

DISCUSSION

Prior research has shown that both AMPK and GIV play integral roles in the preservation of epithelial cell polarity. AMPK has been shown to regulate tight junction stability and its activity is associated with prevention of junction disassembly in low calcium conditions (Zheng and Cantley, 2007). Likewise, GIV has proven to be necessary for normal tight junction formation during epithelial cell development and continued membrane barrier function in cells that have been exposed to low calcium (Sasaki *et al*., 2015). Until now, there has been no connection between these two proteins and their roles in polarity. By identifying GIV as a key substrate of AMPK, and the essential role of this phospho-event in stabilization of cell-cell junctions during energetic stress, this project establishes a novel link between GIV-dependent signaling and AMPK-dependent metabolic sensing in the regulation of epithelial cell polarity. GIV is phosphorylated at residue S245 by AMPK during polarization and under metabolic stress conditions in order to preserve junctional integrity and epithelial cell polarity (**Figure 11**). When phosphorylation at S245 is disrupted, cells are prone to lose junctional stability in stress conditions. This results in a loss of polarity and anchorage independent growth, which eventually may lead to tumorigenesis (**Figure 11**).

In order to better understand the nature of this interaction, it may be useful to ask why AMPK is involved in the regulation of polarity. AMPK is primarily known as a metabolic sensor that functions to increase intracellular ATP when a cell is in need of energy. Therefore, it may seem odd that AMPK is activated during epithelial cell polarization and maintenance, since these are energy-utilizing processes. A possible explanation for this is that polarity is a crucial factor in the proper function and survival of

epithelial cells, and therefore AMPK works to maintain polarity even in conditions of metabolic stress (Hardie, 2011). Another explanation may involve AMPK's role as a tumor suppressor. Since normal epithelial cell polarity plays a role as a non-canonical tumor suppressor by preventing excessive proliferation as well as anchorage-independent growth and invasiveness, AMPK may carry out its own tumor suppressive functions by maintaining polarity in stress conditions.

It is worth noting that LKB1/PAR4 is known as an inhibitor of PAR3 via its activating phosphorylation of PAR1. Therefore, one might assume that other downstream kinases of LKB1 would fulfill similar activities that inhibit apical regulator protein function. However, researchers have found that AMPK actually acts to positively regulate apical polarity through its effects on tight junctions. Our research on the AMPK-GIV interaction seems to confirm this role for AMPK. These findings suggest a more nuanced role for LKB1 as not just a basolateral polarity regulator, but a master regulator of multiple aspects of apical-basal polarity.

The specific method by which GIV pS245 regulates junctional stability and polarity is not entirely clear either. The role of the phosphorylation at S245 is not known as yet; it is possible that this phosphorylated residue causes some sort of conformational change in GIV that allows it to bind to proteins at the junctions or perhaps it is a localization signal that causes GIV to be transported to cell contact sites. However, previous research does show that a pool of GIV binds with PAR-3 and Gαi at cell contact sites during epithelial cell development, and there is evidence that GIV interacts with filamentous actin associated with tight junctions and adherens junctions in order to strengthen them. In fact, overexpression of WT GIV in PAR3 knockdown cells caused a recovery of disrupted actin

organization at cell-cell contact sites and tight junction structures (Sasaki *et al*., 2015). Interestingly, AMPK has been found to phosphorylate cingulin, a tight junction protein, which then recruits tubulin to these junctions (Yano *et al*., 2013). GIV may interact with these tubulin fibers at tight junctions via its HOOK domain at the N-terminus in order to provide stability as polarization occurs.

Regardless of the specific mechanism by which GIV pS245 affects junctions and polarity, it does seem to play a role in two distinct aspects of polarity: the process of epithelial cell polarization during development and the recovery of polarized structure during and after stress conditions. Essentially, these patterns of GIV pS245 localization to cell-cell contact sites and junctions suggest that it is involved in dynamic processes of polarization; GIV pS245 may be at the junctions to provide stability during sensitive periods of change in polarity. Additionally, cross-sections of Z-stack images obtained through confocal microscopy revealed strong colocalization of GIV pS245 and occludin, indicating an interaction between GIV and tight junctions.

While immunofluorescence images of parental MDCK cells were useful in observing the localization patterns of GIV pS245, imaging of stably transfected GIV S245 mutants in MDCK cells under similar conditions unveiled more about the role of this protein in polarity. GIV SA mutant cells consistently showed decreased tight junction protein signal during EGTA and glucose starvation treatments when compared to WT and SD cells. This indicated that a permanent lack of phosphorylation on the S245 site during stress conditions is detrimental to junctional stability and polarity. Furthermore, extended EGTA treatment of these cells showed that WT cells eventually experienced a loss of confluency and decreased tight junction protein localization to cell-cell contact sites similar

to SA cells. However, SD cells maintained their tight junctions and remained confluent, indicating that a constitutive phosphorylation at S245 may prevent prolonged stress induced loss of polarity. We plan to follow up on these experiments by investigating the state of junctions in these MDCK stable cells during recovery after a period of stress. We would expect such experiments to show WT and SD cells recovering more quickly than SA and LP cells based on our previous recovery TEER data in the MDCK stable cell lines.

TEER experiments with the WT, SA, and SD mutants further elucidated the role of pS245 GIV in the function of tight junctions during and after stress. During EGTA treatment, WT cells experienced a significantly larger decrease in resistance compared to SD cells, indicating that the constitutive phosphorylation at this site was assisting the cells in resisting stress-induced junctional instability. Conversely, during a recovery period after EGTA treatment, WT cells displayed a faster increase in resistance when compared to SA and LP cells. Here, the potential for phosphorylation at S245 played an important role in quickly recovering membrane barrier function.

Our research shows implications for GIV pS245 in cancer development as well. The GIV L249P mutant seems to lack the ability to bind to AMPK with the same affinity as WT GIV. As a result, our in vitro kinase assay and IP results indicated that activated AMPK can phosphorylate S245 to a much greater degree on WT versus LP GIV. To begin studying the effect of this mutant on epithelial tissue structure and tumorigenesis, we performed 3D cyst growth assays on our stably transfected MDCK cells, this time including the LP mutant. SA and LP mutant cells exhibited nonspherical structure, multiple lumens, and abnormally large cyst size. All these results suggest a loss of polarity and subsequent aberrant proliferation, resulting in abnormal epithelial tissue structure.

After seeing the effects of these mutants on polarity in normal epithelial cells, we then established a role for GIV pS245 in cancer. 3D tumor growth assays and NIH3T3 transformation assays in stably transfected DLD1 cells both showed that SA and LP mutant cells exhibited the most anchorage independent growth and proliferation. Meanwhile, the SD mutant cells displayed the smallest growths. 2D colony formation assays actually showed opposite growth patterns, with SD cells consistently showing the most growth and SA and LP cells growing the least. These results suggest that GIV pS245 must be an important factor for anchorage-dependent growth. Many untransformed cells require adherence and the greater surface area that accompanies this adherence in order to grow and divide, while transformed cells often exhibit the ability to proliferate without adherence (Assoian, 1997). These results therefore support our claim that GIV pS245 plays a tumor suppressive role. This interpretation makes sense in light of the fact that its upstream kinase, AMPK, acts as a tumor suppressor by preserving polarity and therefore preventing aberrant cell proliferation and migration.

Further research is needed in order to determine GIV pS245's exact role in polarity and tumor suppression. As previously mentioned, it is unclear exactly how the phosphorylation at GIV S245 regulates polarity. We next plan to look into interactions between WT and mutant GIV pS245 and different tight junction associated proteins, since our Z-stack cross section images indicate that this is the primary site of interaction when GIV pS245 localizes to cell contact sites. Based on what is known about GIV's domains, binding to filamentous actin or microtubules associated with these junctions may serve as the connection. Additionally, we have an IF result showing that SA cells exhibit greater levels of actin remodeling than WT and SD cells after glucose deprivation (**Figure 5B**).

This may indicate that GIV pS245 does interact with tight junctions through filamentous actin, and a lack of this phosphorylation disrupts the interaction and allows dysregulation of actin organization, further contributing to depolarization.

An additional player in GIV pS245's role at tight junctions during polarity may be PAR3. Although this project started out of an interest in connecting AMPK and GIV via their roles in polarity through PAR proteins, subsequent research by Ohara and colleagues has shown that PAR3 binds to GIV at its C-terminus, far downstream of the S245 site (Ohara *et al*., 2012). However, binding assays performed by this group have not ruled out other sites of interaction between the two proteins or focused on the potential role of other domains on GIV in regulating this interaction. It is possible that S245 phosphorylation fulfills this type of regulatory function. We therefore plan to further investigate this potential interaction between PAR3 and GIV pS245.

The findings described here take us one step closer to understanding the intricacies of cell polarity. However, there is the potential to learn much more about the role of AMPK and GIV pS245 in both epithelial cell polarity and cancer. Our research makes a novel connection between metabolic stress and polarity regulation, with implications for tumor development. With further research, manipulation of the phosphorylation at this residue could be utilized in treating diseases that result from loss of polarity, including epithelial cancers.

REFERENCES

Assoian R.K. (1997). Anchorage-dependent Cell Cycle Progression. JCB. *136(1),* 1-4.

Bhandari D., Lopez-Sanchez I., To A., Lo I., Aznar N., Leyme A., Gupta V., Niesman I., Maddox A.L., Garcia-Marcos M., Farquhar M.G., Ghosh P. (2015). Cyclin-dependent kinase 5 activates guanine nucleotide exchange factor GIV/Girdin to orchestrate migration-proliferation dichotomy. PNAS. Published online before print. DOI: 10.1073/pnas.1514157112.

Banko M.R., Allen J.J., Schaffer B.E., Wilker E.W., Tsou P., White J.L., Villen J., Wang B., Kim S.R., Sakamoto K., Gygi S.P., Cantley L.C., Yaffe M.B., Shokat K.M., Brunet A., (2011). Chemical Genetic Screen for AMPKα Substrates Uncovers a Network of Proteins Involved in Mitosis. Molecular Cell. *44(6)*. 878-892.

Cardozo T., Totrov M., Abagyan R. (1995). Homology modeling by the ICM method. Proteins. *23(3),* 403-414.

Ellenbroek S., Iden S., and Collard J.G. (2012). Cell polarity proteins and cancer. Elsevier Seminars in Cancer Biology. *22(3),* 208-215.

Enomoto A., Murakami H., Asai N., Morone N., Watanabe T., Kawai K., Murakumo Y., Usukura J., Kaibuchi K., Takahashi M. (2005). Akt/PKB Regulates Actin Organization and Cell Motility via Girdin/APE. Developmental Cell. *9(3),* 389-402.

Ewing R.M., Chu P., Elisma F., Li H., Taylor P., Climie S., McBroom-Cerajewski L., Robinson M.D., O'Connor L., Li M., Taylor R., Dharsee M., Ho H. , Heilbut A., Moore L., Zhang S., Ornatsky O., BukhmanY.V., Ethier M., Sheng Y., Vasilescu J., Abu-Farha M., Lambert J., Duewel H.S., Stewart I.I., Kuehl B., Hogue K., Colwill K., Gladwish K., Muskat B., Kinach R., Adams S., Moran M.F., Morin G.B., Topaloglou T., Figeys D. (2007). Large-scale mapping of human protein-protein interactions by mass spectrometry. Mol Syst Biol. *3(89),* DOI: 10.1038/msb4100134.

Ghosh P., Beas A.O., Bornheimer S.J., Garcia-Marcos M., Forry E.P., Johannson C., Ear J., Jung B.H., Cabrera B., Carethers J.M., Farquhar M.G. (2010). A G{alpha}i-GIV molecular complex binds epidermal growth factor receptor and determines whether cells migrate or proliferate. Mol Biol Cell. *21(13),* 2338-2354.

Ghosh P., Garcia-Marcos M., Farquhar M.G. (2011). GIV/Girdin is a Rheostat which Fine-tunes Growth Factor Signals During Tumor progression. Cell Adhesion and Migration. *5(3),* 237-248.

Goldstein B., Macara I.G. (2007). The PAR proteins: fundamental players in animal cell polarization. Dev Cell. *13(5),* 609-622.

Hardie, D.G. (2011). AMP-activated protein kinase – an energy sensor that regulates all aspects of cell function. Genes and Development. *25*, 1895-1908.

Houssin E., Tepass U., Laprise P. (2015). Girdin-mediated interactions between cadherin and the actin cytoskeleton are required for epithelial morphogenesis in Drosophila. Development. *142*, 1777-1784.

Ichiyama H., Maeda K., Enomoto A., Weng L., Takahashi M., Murohara T. (2012). Girdin/GIV regulates transendothelial permeability by controlling VE-cadherin trafficking through the small GTPase, R-Ras. BBRC. *461(2)*, 260-267.

Johnston D.S., Ahringer J. (2010). Cell Polarity in Eggs and Epithelia: Parallels and Diversity. Cell. *141(5)*, 757-774.

Kalluri R., Weinberg R.A. (2009). The basics of epithelial-mesenchymal transition. J. Clin Investig. *119(6)*, 1420-1428.

Kaplan N.A., Liu X., Tolwinski N.S. (2009). Epithelial Polarity: Interactions Between Junctions and Apical-Basal Machinery. Genetics. *183(3)*, 897-904.

Lee M., Vasioukhin V. (2008). Cell polarity and cancer--cell and tissue polarity as a non-canonical tumor suppressor. J Cell Sci. *121(8)*, 1141-1150.

Lin C., Ear J., Midde K., Lopez-Sanchez I., Aznar N., Garcia-Marcos M., Kufareva I., Abagyan R., Ghosh P. (2014). Structural basis for activation of trimeric Gi proteins by multiple growth factor receptors via GIV/Girdin. Mol Biol Cell. *25(22)*, 3654-3671.

Lizcano J.M., Göransson O., Toth R., Deak M., Morrice N.A., Boudeau J., Hawley S.A., Udd L., Mäkelä T.P., Hardie D.G., Alessi D.R. (2004) LKB1 is a master kinase that activates 13 kinases of the AMPK subfamily, including MARK/PAR-1. EMBO J. *23(4)*, 833-843.

Lopez-Sanchez I., Dunkel Y., Roh Y.S., Mittal Y., De Minicis S., Muranyi A., Singh S., Shanmugam K., Aroonsakool N., Murray F., Ho S.B., Seki E., Brenner D.A, Ghosh P. (2014). GIV/Girdin is a central hub for pro-fibrogenic signalling networks during liver fibrosis**.** Nat Commun. *5*, 4451.

Luo Z., Zang M., Guo W. (2010). AMPK is a metabolic tumor suppressor: control of metabolism and cell growth. Future Oncol. *6(3)*, 457-470.

Marin T.L., Gongol B., Martin M., King S.J., Smith L., Johnson D.A., Subramaniam S., Chien S., Shyy J.Y. (2015) Identification of AMP-activated protein kinase targets by a consensus sequence search of the proteome. BMC Systems Biology. *9(13)*, DOI: 10.1186/s12918-015-0156-0.

Martin-Belmonte F., Perez-Moreno M. (2012). Epithelial cell polarity, stem cells, and cancer. Nature Reviews Cancer. *12*, 23-38.

Mihaylova M.M., Shaw R. (2011). The AMPK signaling pathway coordinates cell growth, autophagy and metabolism. Nat Cell Biol. *13(9),* 1016-1023.

Nesic D., Miller M.C., Quinkert Z.T., Stein M., Chait B.T., Stebbins C.E. (2010). *Helicobacter pylori* CagA Inhibits PAR1/MARK Family Kinases by Mimicking Host Substrates. Nat Struct Mol Bio. *17(1),* 130-132.

O'Brien L.E., Zegers M.M.P., Mostov K.E. (2002). Building epithelial architecture: insights from three dimensional culture models. Nature Reviews Molecular Cell Biology. *3*, 531-537.

Ohara K., Enomoto A., Kato T., Hashimoto T., Isotani-Sakakibara M., Asai N., Ishida-Takagishi M., Weng L., Nakayama M., Watanabe T., Kato K., Kaibuchi K., Murakumo Y., Hirooka Y., Goto H., Takahashi M. (2012). Involvement of Girdin in the determination of cell polarity during cell migration. PLoS One. *7(5),* e36681.

Sasaki K., Kakuwa T., Akimoto K., Koga H., Ohno S. (2015). Regulation of epithelial cell polarity by PAR-3 depends on Girdin transcription and Girdin-Gαi3 signaling. J Cell Sci. 128(13), 2244-2258.

Stein M.P., Wandinger-Ness A., Roitbak T. (2002). Altered trafficking and epithelial cell polarity in disease. TRENDS in Cell Biology. *12(8),* 374-381.

Yano, T., Matsui T., Tamura A., Uji M., Tsukita S. (2013). The association of microtubules with tight junctions is promoted by cingulin phosphorylation by AMPK. J Cell Biol. *203(4),* 605-614.

Zhang L., Li J., Young L.H., Caplan M.J. (2006). AMP-activated protein kinase regulates the assembly of epithelial tight junctions. Proceedings of the National Academy of Sciences. *103(46),* 17272-17277.

Zheng B., Cantley L.C. (2007). Regulation of epithelial tight junction assembly and disassembly by AMP-activated protein kinase. Proceedings of the National Academy of Sciences. *104(3),* 819-822.

Zhou H., Di Palma S., Preisinger C., Peng M., Polat A.N., Heck A.J., Mohammed S. (2013). Toward a comprehensive characterization of a human cancer cell phosphoproteome. J Proteome Res. *12(1),* 260-271.